DOI:
10.1093/toxsci/kfv232

Document Version
Peer reviewed version

Transcriptional Profiling of Dibenzo[*def,p*]chrysene-induced Spleen Atrophy Provides Mechanistic Insights into its Immunotoxicity in Muta^{TM}Mouse

Nikolai L. Chepelev,[*] Alexandra S. Long,[*] Andrew Williams,[*] Byron Kuo,[*] Rémi Gagné,[*] Dean A. Kennedy,[*] David H. Phillips,[†] Volker M. Arlt,[†] Paul A. White,[*] and Carole L. Yauk[*,1]

[*]Environmental Health Science and Research Bureau, Healthy Environments and Consumer Safety Branch, Health Canada, Ottawa, Ontario, K1A 0K9, Canada; [†]Analytical and Environmental Sciences Division, MRC-PHE Centre for Environment and Health, King's College London, London SE1 9NH, UK

[1]To whom correspondence should be addressed at Environmental Health Science and Research Bureau, Health Canada, Environmental Health Centre, Tunney's Pasture, Ottawa, ON, K1A 0K9 Canada. Fax: 613-941-8530. E-mail: Carole.Yauk@hc-sc.gc.ca.

Abstract

Dibenzo[*def,p*]chrysene (DBC) is the most carcinogenic polycyclic aromatic hydrocarbon (PAH) examined to date. We investigated the immunotoxicity of DBC, manifested as spleen atrophy following acute exposure of adult Muta™Mouse males by oral gavage. Mice were exposed to 0, 2.0, 6.2, or 20.0 mg DBC /kg-bw per day, for three days. Genotoxic endpoints (DBC-DNA adducts and *lacZ* mutant frequency in spleen and bone marrow, and red blood cell micronucleus frequency) and global gene expression changes were measured. All of the genotoxicity measures increased in a dose-dependent manner in both tissues. Gene expression analysis showed that DBC activates p53 signalling pathways related to cellular growth and proliferation, which was evident even at the low dose. Strikingly, the expression profiles of DBC exposed mouse spleens were highly inversely correlated with the expression profiles of the only published toxicogenomics dataset of enlarged mouse spleen. This analysis suggested a central role for Bnip3l, a pro-apoptotic protein involved in negative regulation of erythroid maturation. RT-PCR confirmed expression changes in several genes related to apoptosis, iron metabolism, and aryl hydrocarbon receptor signalling that are regulated in the opposite direction during spleen atrophy versus benzo[*a*]pyrene-mediated splenomegaly. In addition, benchmark dose modeling of toxicogenomics data yielded toxicity estimates that are very close to traditional toxicity endpoints. This work illustrates the power of toxicogenomics to reveal rich mechanistic information of immunotoxic compounds and its ability to provide information that is quantitatively similar to that derived from standard toxicity methods in health risk assessment.

Key Words: human health risk assessment, mode of action, benchmark dose modeling, spleen.

INTRODUCTION

Polycyclic aromatic hydrocarbons (PAHs) are present as mixtures in many complex matrices, including petroleum, industrial emissions, cigarette smoke, smoked foods, municipal waste waters and airborne emissions from the internal combustion engines and waste incinerators (reviewed in (White, 2002)). Dibenzo[*def,p*]chrysene (DBC; formerly known as dibenzo[*a,l*]pyrene) is the most carcinogenic PAH (Nakatsuru *et al.*, 2004). It has been suggested that its higher carcinogenic potency arises due to the higher reactivity of its diol epoxide metabolites towards DNA compared to the metabolites of other PAHs, resulting in a greater extent of DNA damage (reviewed in (Bolstad *et al.*, 2003,Committee on Carcinogenicity of Chemicals in Food, Consumer Products and the Environment, 2003)]). In addition, due to molecular geometry (steric hindrance), the ultimate carcinogenic metabolite of DBC (Fig. 1) preferentially forms DNA adducts at the N^6 rather than N^2 position of deoxyadenosine; N^6 adducts are more resistant to nucleotide excision repair than N^2 adducts that are formed by other PAHs (reviewed by [Harper et al., 2015]). In mice, DBC exposure leads to tumor formation at multiple sites, including lymphomas of the spleen (reviewed in [IARC, 2010]). DBC is considered "possibly carcinogenic" in humans (group 2B) by the International Agency for Research on Cancer (IARC) (IARC Working Group on the Evaluation of Carcinogenic Risks to Humans, 2010). DBC concentration can reach 0.51-1.51 ng/m^3 in ambient air particles, which is comparable to other PAHs such as benzo[*a*]pyrene (BaP) (De Raat *et al.*, 1987). We were unable to find any regulatory guidelines for DBC.

In addition to the renowned carcinogenic activity, multiple studies have documented the immunotoxicity of PAHs (reviewed in (Ramesh *et al.*, 2004)], for example). The immunosuppressive properties of PAHs have been investigated using several assays, including

primary antibody response to sheep red blood cells (also known as the "plaque-forming cell assay" (e.g., (Gao *et al.*, 2005)) and measurement of spleen weight (e.g., (De Jong *et al.*, 1999)). The latter endpoint is measured using an Organisation for Economic Cooperation and Development (OECD) guideline (TG407) (OECD, 2008). The spleen has a highly organized lymphoid compartment and is involved in the removal of blood-borne microorganisms and cellular debris, in the phagocytosis of erythrocytes, and in iron recycling, and is considered the most important organ for antibacterial and antifungal immune reactivity (Mebius and Kraal, 2005). Therefore, spleen size is considered an effective measure of immune response since the spleen plays a primary role in initiating immune responses to blood-borne antigens (reviewed in (Cesta, 2006)).

Previous work has shown that exposure of mice to PAHs leads to both spleen atrophy and splenomegaly, depending on the PAH and the route of exposure. For example, B6C3F1 female mice showed marked reduction in spleen weight and spleen cellularity after a 5-day exposure to 50 and 100 mg/kg-bw per day BaP by intraperitoneal injection (Holladay and Smith, 1995). Similar reductions in spleen weight were reported in adult female C57BL/6N mice gavaged with 50 and 150 mg/kg-bw per day of 7,12-dimethylbenz[*a*]anthracene (DMBA) for 5 days (Gao *et al.*, 2005). In contrast, splenomegaly was observed in female NZB/WF1 mice that received BaP *via* dermal exposure for 30 days at 20 mg/kg-bw per day (Booker and White, 2005).

Although the exact mechanisms underlying the splenic effects of PAHs remain to be elucidated, several molecules have been implicated as mediators of DBC- and DMBA-associated immunotoxicity (reviewed in (Gao and Burchiel, 2014)). In particular, spleen atrophy is p53-dependent, as no effect on the spleen weight was observed in p53-deficient C57BL/6N female mice exposed to 17, 50, or 150 mg/kg-bw per day DMBA for 5 days, but not in wild-type exposed mice (Gao *et al.*, 2008). DMBA mediates p53 activation by p53 phosphorylation and

nuclear accumulation in the murine spleen, which does not happen in mice lacking cytochrome 450 1B1 (*Cyp1b1*) and microsomal epoxide hydrolase (*mEH*) (Gao *et al.*, 2008). It was thus proposed that p53-mediated apoptosis is responsible for DMBA cytotoxicity in the spleen at high doses (Gao *et al.*, 2008), while at lower doses p53-mediated cell cycle arrest may also contribute to dose-dependent decreases in spleen weight (Scott Burchiel, personal communications).

Similarly, DBC exposure is immunotoxic as measured by the plaque-forming cell assay and leads to p53 accumulation in the nucleus of spleen cells isolated from C57BL/6J mice *in vitro* (Li et al., 2010). In addition, DBC is bioactivated by CYP1B1 and mEH enzymes (Fig. 1; reviewed in (Gao and Burchiel, 2014)) to form immunotoxic reactive intermediates ((Shimada and Fujii-Kuriyama, 2004)). Interestingly, the aryl hydrocarbon receptor (AHR), which mediates PAH-inducible expression of phase I and II metabolism genes including CYP1B1, appears to be dispensable for DMBA-mediated immunotoxicity in mouse spleen (Gao *et al.*, 2008). Therefore, it is currently hypothesized that low, constitutive levels of CYP1B1 are sufficient for DMBA bioactivation in the spleen (Gao and Burchiel, 2014).

The objectives of this project were two-fold: *i*) to investigate the mechanisms involved in PAH-induced immunotoxic effects in mouse spleen using toxicogenomic tools; and *ii*) use this mechanistic information to compare toxicogenomics and traditional toxicity (apical) data in order to investigate the potential utility of toxicogenomics in human health risk assessment of immunotoxic compounds.

MATERIALS AND METHODS

Animal treatments. Adult male Muta™Mouse (strain 40.6; a transgenic mouse harboring bacteriophage lambda shuttle vector and frequently used in mutation research, described

elsewhere (Gossen *et al.,* 1989), 9 weeks of age) were individually housed in a microVENT ventilated rack (Allentown Inc., Allentown, NJ) on a 12 h light/12 h dark cycle. Mice were bred, maintained, and treated in accordance with the Canadian Council for Animal Care Guidelines and all mouse work was approved by Health Canada's Animal Care Committee. Mice received standard rodent chow (2014 Teklad Global standard rodent diet) and water *ad libitum* for the duration of the study. Mice were administered DBC (CAS no. 191-30-0, purity ≥ 98%, Cambridge Isotopes, Tewksbury, MA) dissolved in highly refined olive oil (Sigma-Aldrich, Oakville, ON, Canada) at 0.005 ml/g body weight. The doses (2.0, 6.3, and 20.0 mg/kg-bw per day) were administered by oral gavage for three consecutive days. Doses were selected based on preliminary dose range-finding work that showed a significant reduction in body weight exceeding 10%, paleness in the liver, as well as bone marrow cytotoxicity at doses above 5 mg/kg-bw per day (administered daily for 28 days). Significant spleen reduction was observed in animals treated for 3 consecutive days with doses above 25 mg/kg-bw per day. There were 15 animals in each dose group (5 harvested per each of 3 time points [i.e., 4, 24, and 72 h after the last exposure]), as well as in the vehicle control groups. Five mice from each dose group (and control group) were anesthetized using isoflurane gas and then euthanized via cervical dislocation followed by chest cavity opening 4, 24, or 72 h after the final dose. For the 72-h dose group, peripheral blood was collected from the facial vein 48 h after the last dose for micronucleus analysis following OECD guideline # 474 (OECD, 1997). For all time points, the spleen was removed, flash-frozen in liquid nitrogen, and stored at -80°C. To provide mechanistic insights into the "opposite" phenotype, splenomegaly, we used spleens from male mice of the same strain that were dosed with 0 or 100 mg BaP/kg-bw per day for 28 days (as described in Malik *et al.*, 2012) and sacrificed 88 days after the last treatment.

Genomic DNA isolation for mutation and DNA adduct analyses. Frozen spleen samples were minced and combined with 5-ml ice cold lysis buffer (1 mM Na_2EDTA, 100 mM NaCl, 20 mM Tris-HCl, pH 7.4), supplemented with 1% SDS (w/v) and 0.1 mg/ml RNase A, and incubated at 37˚C overnight with gentle shaking. Genomic DNA was then isolated using a phenol/chloroform extraction procedure described previously (Douglas *et al.*, 1994; Vijg and Douglas 1996). Isolated DNA was dissolved in 100 µl TE buffer (10 mM Tris pH 7.6, 1 mM EDTA) and stored at 4˚C until use.

DNA adduct analysis. The nuclease P1 digestion enrichment version of the ^{32}P-postlabelling assay was used to measure DNA adduct frequency. The procedure was performed as described (Wohak *et al.*, 2014,Phillips and Arlt, 2007,Siddens *et al.*, 2012).

Mutant frequency analysis. The PGal (phenyl-β-D-galactoside) positive selection assay was used to assess the *lacZ* mutant frequency in DNA samples isolated from spleen from the 72-h post-exposure group only, as previously described (Lambert *et al.*, 2005; Vijg & Douglas, 1996; Lemieux *et al.*, 2011). Mutant frequency was calculated as the ratio of mutant plaque forming units (i.e., pfu) to total pfu, and analysis of mutant frequency data was performed as described previously (Lemieux *et al.*, 2011).

Peripheral blood micronucleus analysis. As indicated above, ~60-100 µl of blood was collected from the facial vein from the 72-h post-exposure group, 48 h after the last exposure, according to OECD guideline #474 (OECD, 1997). Blood samples were processed and fixed according to MicroFlow kit instructions (Litron Laboratories, Rochester, NY). Coded samples were shipped to Litron Laboratories for analysis of micronucleus (MN) frequency in reticulocytes (RETs) and normochromatic erythrocytes (NCEs). Samples were analyzed and

stained according to (Dertinger *et al.,* 2004). Frequencies of MN-RET, MN-NCE, as well as % RET were determined for all dose groups, with the exception of the high dose where the % RET was too low to score MN-RET frequency.

Dihydro-8-oxo-2'-deoxyguanosine (8-oxo-dG) analysis. DNA was extracted by the DNAzol method as it produces minimal amounts of artificial DNA oxidation (Mangal *et al.*, 2009), as described elsewhere (Chepelev *et al.,* 2015c). Approximately 15 mg of spleen was used (N=5, 4- and 24-h post-exposure samples). Extracted DNA pellets were dissolved in 21 µL of Chelex 100 resin-treated 50 mM dibasic sodium phosphate buffer (pH 7.4) containing 50 mM $MgCl_2$ and 1 mM desferal and digested with 1 unit of DNase I (type II, from bovine pancreas, Sigma-Aldrich, ON, Canada) for 1.5 h at 37°C. The pH was adjusted to 8.6 with 5 mM sodium phosphate dibasic buffer and the mixture was digested with 0.025 units of Phosphodiesterase I (type II from *Crotalus adamaneus* venom, Sigma-Aldrich) for 1.5 h at 37°C. Finally, the mixture was digested with 0.4 units of alkaline phosphatase (type III from *Escherichia coli*, Sigma-Aldrich) for 1.5 h. Methanol was added to the digest to a final concentration of 6%. The digest was stored at –80°C until HPLC analysis. A Waters 2690 Alliance HPLC system with a glassy carbon electrochemical detector and YMC-BASIC column were used for the analysis. Fifty millimolar phosphate buffer (pH 6.2) containing 6% methanol and 2 mM KCl served as the mobile phase. The voltage for 8-oxo-dG detection was +0.5 V and +0.9 V for 2'-deoxyguanosine detection; the flow rate was 1 mL/min. Results are expressed as 8-oxo-dG/2'-deoxyguanosine ratio.

Immunoblot analysis. Approximately 50 mg of spleen from control and high dose samples collected 4 h and 24 h post-exposure was lysed by shaking with a metal bead for 10 min at 25 Hz in 1 mL of isotonic buffer (25 mM HEPES, 5 mM $MgCl_2$, 1 mM EGTA, pH 7.5). Equal amounts of protein (20-30 mg, determined by BCA assay (Pierce Biotechnology, Rockford, IL, USA))

were loaded per lane on 4–15% Mini-PROTEAN® TGX™ pre-cast gels (Bio-Rad Mississauga, ON) and run for 1 h at 120 V. Protein was transferred onto Immobilon-P PVDF membrane (Millipore, Billerica, MA, USA) at 120 V for 1 h, blocked with 5% non-fat dry milk in phosphate buffered saline containing 0.1% Tween 20 for 1 h and probed with rabbit monoclonal BNIP3L antibody (Abcam, Cambridge, MA, USA, cat.no. EPR4033, 1:1000 dilution) or beta-actin antibody (Cell signalling, Danvers, MA, USA, cat. no. 4970, 1:5000 dilution) for 1 h. Signal was visualized by probing with horse radish peroxidase-conjugated goat-anti rabbit polyclonal antibody (Assay designs, Ann Arbor, MI, USA, cat. no. SAB-300), chemiluminescence substrate (Millipore), and scanning with ChemiDoc XRS+ (Bio-Rad). Images were analyzed using AlphaEaseFC software version 3.1.2 (Alpha Innotech/Cell Biosciences, Santa Clara, CA). Results are expressed as relative band density compared to control, normalized to beta-actin expression.

Total RNA isolation, microarray hybridization, and gene expression analysis. RNA was isolated, hybridized, and analyzed as described elsewhere (Malik *et al.*, 2013,Jackson *et al.*, 2014). Samples with RNA integrity numbers above 6.0 (Agilent Bioanalyzer, Agilent Technologies, Mississauga, ON, Canada) were hybridized to Agilent 8x60 K whole genome microarrays. Agilent Feature Extraction Software (version 11) was employed for data extraction and the complete dataset has been deposited in the Gene Expression Omnibus (http://www.ncbi.nlm.nih.gov/geo/, accession number GSE72334). Normalization using locally weighted scatterplot smoothing (LOWESS) (Yang *et al.*, 2002) in R (R-Development-Core-Team, 2010), determination of differential gene expression by microarray analysis of variance (MAANOVA) (Wu *et al.*, 2003), and calculation of false-discovery rate- (FDR) adjusted p-values were carried out as described elsewhere (Jackson *et al.*, 2014).

Real-time quantitative reverse transcription polymerase chain reaction (RT-PCR). A custom RT-PCR array, containing proprietary probes (Qiagen) was designed to validate microarray results. PCR arrays were run on a CFX96 real-time detection system (Bio-Rad). C_t values were normalized to *Gapdh* and gene expression was analyzed on-line at: http://pcrdataanalysis.sabiosciences.com/pcr/arrayanalysis.php.

Ion Proton™ Sequencing (RNA-Seq). Next-generation sequencing of eight spleen samples (control vs. high dose, 4 h after the last treatment, N=4) and 14 bone marrow samples (N=4 for control, low, and medium dose, and N=2 for high dose, 24 h post-treatment) was carried out using an Ion Proton™ sequencer (Life Technologies. Carlsbad, CA). Only one dose and time point was profiled for the spleen in order to confirm microarray results, while for the bone marrow, three doses were processed as no other toxicogenomics data were generated for this tissue. Poly-A RNA enrichment (DynaBeads® mRNA DIRECT Micro Kit) was performed for each spleen sample on 2.5 µg of total RNA. Ribosomal RNA removal (RiboMinus™ Eukaryote System v2) was performed for each bone marrow sample on 2.5 µg of total RNA. The Ion Total RNA-Seq Kit and AB Library Builder™ (option 1; whole transcriptome (Ion Total Library Version 1.0)) were used to fragment and prepare the sample libraries from poly-A enriched samples. The 3'-end barcode adapters provided in the Ion Xpress™ RNA-Seq Barcode 1–16 Kit Automated Library Construction kit were ligated to the ends of the fragmented libraries (each PCR product receiving its own unique barcode). Libraries were then amplified using the Platinum® PCR SuperMix High Fidelity. Each amplified library was quantified/qualified using the Agilent® High Sensitivity DNA Kit and Agilent® Bioanalyzer® 2100 Instrument. Aliquots of each library were pooled together for a total final concentration of 16 pM. Emulsion PCR (em-PCR) of the pooled libraries was done using Ion Sphere™ particles on the Ion OneTouch™

2 system. The Ion OneTouch™ ES was used to enrich for particles containing em-PCR products and the Qubit® 2.0 Fluorometer was used to assess the quality of enrichment. Enriched particles were deposited into the wells of an Ion P1™ chip (version 1) and sequenced by semi-conductor sequencing.

The Proton™ Torrent Server version 4.0.2 interpreted the sequencing data and generated FASTQ files for each barcoded sample. Reads were trimmed to remove low quality read prefixes and suffixes, then aligned to the reference genome (GRCm38) using Star (Dobin *et al.*, 2013) and Bowtie (Langmead and Salzberg, 2012). Following alignment, gene counting was performed with HT-Seq count (http://www-huber.embl.de/users/anders/HTSeq/doc/count.html) with the m parameter set to "intersection-nonempty" using the Ensembl GTF annotation (GRCm38v72). The table of counts was then imported into R where genes with a total count less than one read per million reads were removed from further analyses. The EdgeR (Robinson *et al.*, 2010) package was used for the analysis by normalizing with TMM (Robinson and Oshlack, 2010) and calculating differentially expressed genes using the exactTest function. The data is publically available from Sequence Read Archive (SRA, http://www.ncbi.nlm.nih.gov/ SRA submissions: SRP062701 (spleen) and SRP062765 (bone marrow)).

Bionformatic analyses. All genes with the FDR $P \leq 0.05$ and fold change ≥ 1.5 were uploaded into Ingenuity Pathway Analysis™ (IPA™, Ingenuity Systems, Redwood City, CA, USA) and NextBio™ (http://nextbio.com) to identify biological pathways, functions, or processes that are affected in the spleen by DBC exposure. IPA employs Fisher's exact tests to examine the significance of the association between a given dataset and the canonical pathways and functions as defined by IPA™. NextBio™ compares the input dataset to curated datasets to identify published cases of mouse models with similar gene profiles in the spleen. The meta-

analysis function was used to gain further insight into DBC-mediated immunotoxicity. The significance of negative or positive correlations between the query and curated datasets is assessed in NextBio™, taking into account a number of factors, most notably, directionality and strength of the overlap/enrichment between the two datasets (Kupershmidt *et al.*, 2010).

Benchmark dose (BMD) modeling. Gene expression and apical data were analyzed using BMDExpress (Yang *et al.*, 2007), as we described previously (Moffat *et al.*, 2015). The probes were fitted to each of the Hill, Power, Linear and Polynomial 2° models, with the following parameters: maximum iterations of 250, BMR factor of 1.349, confidence level of 0.95 and power restricted to ≥ 1. A best-fit model was selected based on: 1) the nested chi-square test cut-off p-value of 0.05 to select between Linear and Polynomial models; 2) the lowest Akaike Information Criterion (AIC) to select between Hill and Power models; and 3) the goodness-of-fit p-value for likelihood ratio test of > 0.05. In the case that the k parameter was less than 1/3 of the lowest positive dose, the Hill model is flagged, and the next best fit model was selected if it had a goodness-of-fit p-value > 0.05. In addition, BMD values were generated for the IPA canonical pathways and for the "Cellular growth and proliferation, hematological system development and function, hematopoiesis top diseases & function" IPA network since it was the only network that could be described by the genes that were affected by DBC at all doses and all time points (seven and ten genes for 4- and 24-h time points, respectively. In addition, BMDs were derived for the gene *Cdkn1a*using both DNA microarray (derived in BMDExpress) and RT-PCR because of its established association with DNA damage response (Li *et al.*, 2015). The individual gene expression (delta Ct values from RT-PCR) data for *Cdk1na* were analyzed as described elsewhere (Chepelev *et al.*, 2015a). Briefly, the US EPA's BMDS software version 2.50, with the patched continuous polynomial model and Wizard Output Report (described at:

http://www.epa.gov/ ncea/bmds/), was used. Gene expression (delta Ct) values were fit against five continuous (linear, polynomial, power, Hill, and exponential) dose-response models and the best model was selected based on the lowest Akaike's information criterion, provided that chi-square goodness of fit p-value was > 0.1. The default BMDS 2.50 settings were used to obtain the BMD_{1SD} and their lower 95% confidence limit ($BMDL_{1SD}$) values.

Statistical analyses for lacZ, MN, and DNA adducts. The *lacZ*, MN, and DNA adduct data were analyzed using SAS software, Version 9.1 of the SAS System for Windows (© 2002-2010 by SAS Institute Inc, Cary, NC) by Poisson regression. The data were fit to the model $\log(E(Yi)) = \log ti + \beta xi$, where E(Yi) is the expected value for the ith observation, β is the vector of regressions coefficients, xi is a vector of covariates for the ith observation, and ti is the offset variable used to account for differences in observation count period (i.e., pfu). The offset (i.e., natural log of pfu) was given a constant coefficient of 1.0 for each observation, and log-linear relationships between mutant count and test article concentration were specified by a natural log link function. Type 1, or sequential analysis, was employed to examine the statistical significance of the chemical treatment.

Other statistical analyses. Spleen and liver weights were analyzed by one–way ANOVA in Microsoft Excel. The liver somatic index, spleen somatic index, and 8-oxodG data were analyzed in R. An ANOVA was conducted to determine whether there was a treatment effect, and post-hoc comparisons of each dose with control samples were then employed using the Tukey honest significant difference test. Scrutiny of the residuals revealed that all data met the assumptions of homogeneity of variance and normality; therefore, no data transformations were required. Immunoblotting results (band densitometry values converted to fold-change in the high dose over control) for Bnip3l were analyzed using the unpaired t-test function in Microsoft Excel.

RESULTS

General and organ-specific response of Muta™Mouse to DBC

Mice exposed to three consecutive doses of 2.0, 6.3, or 20.0 mg/kg-bw per day DBC displayed no overt signs of toxicity as assessed by standard serum chemistry screens; the only significant effects noted were a ~2-fold reduction in serum triglycerides at the medium dose, and a ~25% decrease in serum blood urea nitrogen 4 and 24 h after the last treatment, respectively (data not shown). There was no overall weight loss compared to the control group. However, the mice displayed profound loss of spleen weight (i.e., somatic index or % body weight) that was greatest at the high dose 72 h post-treatment (over 40% loss, Fig. 2). No changes were observed in the weight of the livers (Supplementary Fig. 1) or any other organs (data not shown).

DNA adducts as indicators of DBC metabolism and tissue exposure

DNA adducts were measured in the spleen and bone marrow by ^{32}P-postlabeling analysis. There was a dose-dependent increase in the levels of DBC-DNA adducts across all concentrations and time points in both spleen and bone marrow (Fig. 3). The main adducts were derivatives of the DBC metabolite DBC-11,12-diol-13,14-epoxide (Wohak *et al.,* 2014) and representative autoradiograms of the obtained DNA adduct profiles are shown in Supplementary Fig. 2. No adducts were detectable in DNA isolated from control (untreated) animals. The spleen had roughly 2-fold higher levels of adducts than the bone marrow. There was a clear decrease in the adduct levels from 4 to 72 h in the bone marrow that was most pronounced at the high dose (Fig. 3B); on the contrary, there was over a two-fold increase in adduct levels at the highest dose from 4 to 24 h in the spleen (Fig. 3A).

LacZ mutant frequencies in spleen and bone marrow

Mutant frequency for the *lacZ* transgene was evaluated in the spleen and bone marrow 72 h after the last exposure (Fig. 4). Despite 2-fold higher adduct levels in the spleen (Fig. 3), bone marrow had much higher mutant frequencies, reaching over 10-fold increases above controls for the high dose (Fig. 4). In contrast to the bone marrow, a consistent dose-response for induced mutant frequency in the spleen was not observed.

Circulating reticulocytes and micronucleus formation

Micronucleus formation was measured in peripheral blood collected 46 h after the last exposure by flow cytometry (Dertinger *et al.,* 2004). The approach exploits cell-surface markers that enable the analysis of newly-formed erythrocytes (i.e., RETs) that are less than 48-h old and mature erythrocytes (i.e., NCEs). There were statistically-significant increases in the formation of both MN-RETs and MN-NCEs (Fig. 5). There was clear dose-response effect for the increase in both MN-NCEs and MN-RETs, but the latter was more pronounced, giving rise to a much steeper slope in the dose-response curve. At the highest dose, the % RET was < 0.03% (Fig. 5B), which is too low to reliably score MN-RET frequency.

DNA oxidation

DNA oxidation in the spleen was quantified using a modified HPLC method that measures an established DNA oxidation marker, dihydro-8-oxo-2'-deoxyguanosine (8-oxo-dG) (Chepelev *et al.,* 2015c). In contrast to the other genotoxicity endpoints (i.e., DNA adducts, *lacZ* mutant frequency, and micronucleus formation), 8-oxo-dG levels increased only at the highest dose and only at the 4 h post-exposure time-point (1.9-fold increase vs. control, Fig. 6).

Gene expression changes in the spleen detected by Agilent microarrays

DBC affected the expression of 45, 361, and 1566 probes at the low, medium, and high doses respectively, 4 h after the last treatment, and 195, 595, and 1204 probes, 24 h after the last treatment (Supplementary Table 1). Hierarchical cluster analysis of all of the differentially expressed genes revealed a clear separation between control and treatment groups (Supplementary Fig. 3). The highest dose was on a separate branch from all other treatments, regardless of time point. Thus, gene expression profiles were primarily affected by dose and demonstrate clear treatment effects as a result of DBC exposure. The complete microarray data set for this study is available through the Gene Expression Omnibus at NCBI (http://www.ncbi.nlm.nih.gov/geo/) under accession number GSE72334.

Eighteen genes were perturbed at all doses and both time points (Table 1). Analysis of these genes in IPA revealed that 11 out of these 18 genes belong to a "cellular growth and proliferation, hematological system development & function, hematopoiesis" network. The 11 genes are: B-cell lymphoma (Bcl2)/adenovirus E1B 19kDa interacting protein 3-like (*Bnip3l*), cyclin-D1-binding protein 1 (*Ccndbp1*), ephrin type-B receptor 6 (*Ephb6*), FCH and double SH3 domains protein 1 (*Fchsd1*), fibroblast growth factor 13 (*Fgf13*), methyl-CpG binding domain protein 5 (*Mbd5*), nuclear receptor coactivator 4 (*Ncoa4*), serine/threonine-protein phosphatase PP1-beta catalytic subunit (*Ppp1cb*), Sry (sex determining region y)-box 13 (*Sox13*), stefin A3 (*Stfa3*), and Yip1 domain family, member 4 (*Yipf4*). Activation of "cell cycle: G2/M DNA damage checkpoint regulation" and inhibition of "cyclins and cell cycle regulation" networks occurred 4 or both 4 and 24 h post-exposure to the high dose, respectively (Table 2), in parallel with reduced gene expression of cyclins A, B, D1, and E. *Cdkn1a* was upregulated by DBC at all doses 4, but not 24 h after the last exposure, consistent with its predicted activation based on the

gene expression of its downstream targets at the medium dose at 4 h, and the medium and high doses 24 hrs post- exposure (Supplementary Table 2).

In addition to p53-mediated cell cycle arrest, DBC exposure affected the expression of genes involved in two other p53 functions: apoptosis (upregulation of Bcl-2-binding component 3 (*Bbc3*, also known as p53 upregulated modulator of apoptosis or PUMA)) and antiapoptosis (downregulation of baculoviral IAP repeat containing 5 (*Birc5*), cyclin B2 (*Ccnb2*), and protein regulator of cytokinesis 1 (*Prc1*)). *Bbc3* was upregulated 24 h post-exposure to the highest dose, whereas *Birc5*, *Ccnb2*, and *Prc1* were downregulated 4 h post-exposure to the highest dose (Supplementary Table 1). *Ccnb2* and *Prc1* were also downregulated 24 h post-exposure to the medium and high doses. In addition to p53, the IPA "upstream activators" application predicted that a number of other transcriptional regulators were affected by DBC in the spleen, including activation of Bnip3l, and inhibition of erythropoietin (Epo) and erythroid transcription factor or GATA-binding factor 1 (Gata-1) (Supplementary Table 2).

Query against curated datasets in NextBio revealed that DBC-induced spleen profiles were strongly negatively correlated with spleen expression profiles from *Bnip3l* knock-out mice (Diwan *et al.,* 2007). Specifically, 634 genes that were upregulated in the spleens of Muta^{TM}Mouse exposed to the high dose of DBC were downregulated in the spleens of mice lacking *Bnip3l* and, conversely, 884 genes that were downregulated in response to DBC were upregulated in the spleens of *Bnip3l* knock-out mice (Fig. 7). Strikingly, *Bnip3l* gene expression was significantly downregulated relative to control at all three doses and time points in our study (Table 1). The *Bnip3l*-deficient mice exhibit the opposite phenotype to spleen atrophy that we report here, i.e., massive splenomegaly, characterized by erythroblast hyperplasia and reduced apoptosis during erythrocyte maturation in the bone marrow and spleen (Diwan *et al.,* 2007). The two opposite

phenotypes are consistent with the opposite pattern of gene expression (negative correlation) between this study and the aforementioned (Diwan *et al.*, 2007) study. Bnip3l is a pro-apoptotic protein that regulates the production of erythrocytes, maintains hematological homeostasis, and affects spleen size (Diwan *et al.*, 2007).

Overview of altered gene expression in the spleen detected by RNA-Seq

RNA-Seq revealed 2465 differentially expressed transcripts at the highest dose 4 h after the last treatment (Supplementary Table 3). Of these, 497 genes were also identified as differentially expressed by the Agilent microarrays. Analysis in IPA revealed that shared probes had disease functions and canonical pathways related to cell cycle, DNA damage, and hematological disease. Both technologies identified "cell cycle", "cellular growth and proliferation", and "cell death and survival" as top molecular and cellular functions perturbed by DBC (Supplementary Fig. 4). Similar to the microarray data, RNA-Seq analysis suggested activation of p53, Cdkn1a, and Bnip3l, and inhibition of Epo and Gata-1.

Validation of gene expression by RT-PCR

Ten genes were selected for validation of microarray results by RT-PCR. The selection was based on the involvement of the genes in the pathways described above. The selected genes were involved in p53-mediated DNA damage response (*Bbc3*, *Birc5*, *Cdkn1a*, and *Prc1*), heme metabolism (ferrochelatase (*Fech*), heme oxygenase (decycling) 1 (*Hmox1*), and AHR-mediated signalling (*Cyp1b1* and NAD(P)H dehydrogenase, quinone 1 (*Nqo1*)). In addition, the expression of mitochondrial fission regulator 1 (*Mtfr1*) and *Bnip3l* was examined by RT-PCR. Table 3 lists expression values obtained by Agilent microarrays for the 10 genes selected for the validation by RT-PCR. All of the ten genes except *Cyp1b1* had expression changes > ±1.5-fold relative to controls and FDR-adjusted p-values < 0.05 on DNA microarrays. *Cyp1b1* expression was just

below a 1.5-fold change (i.e., 1.44 and 1.48-fold increase over control 4 and 24 h after the last treatment, respectively (Table 3)). *Bnip3l* and *Fech* had clear dose-dependent responses for both time points, as did *Birc5* at the 24 h time point.

RT-PCR confirmed the changes in the expression for nine out of 10 genes; alterations in *Hmox1* levels observed using DNA microarrays (Table 3) were not reproduced by RT-PCR (Table 4). In addition, RT-PCR revealed that *Cdkn1a* was upregulated at all doses and time points. RNA-Seq confirmed expression changes following DBC exposure of all perturbed genes with the exception of the relatively low abundant *Cyp1b1* transcript (Table 5). RNA-Seq also detected 2.1-fold upregulation of *Hmox1*.

Confirmation of reduced Bnip3l expression by immunoblotting

Bnip3l expression was analyzed by immunoblotting. Bnip3l may be visualized by immunoblotting as both a monomer and a dimer of approximately 42 and 80 kiloDaltons, respectively (Imazu *et al.,* 1999), which can also be seen in Fig. 8. The expression of Bnip3l dimers for both time points and the Bnip3l monomer for the 24 h time point were significantly reduced at the high dose of 20 mg/kg-bw per day, in agreement with gene expression profiling by microarrays, RT-PCR, and RNA-Seq (Table 5).

Comparison of the expression of selected genes in the PAH-induced models of spleen atrophy versus enlargement

As the pattern of gene expression associated with DBC-induced spleen atrophy was the opposite to what is seen in the spleen of *Bnip3l* knock-out mouse (Diwan *et al.,* 2007), we hypothesized that alteration of spleen size in response to PAH exposure in mice is controlled by a similar set of genes. To this end, we examined the expression of the RT-PCR-validated genes

in the spleens of Muta^{TM}Mouse males that displayed approximately 5-fold increases in spleen weight 88 days after a 28-day exposure to BaP, from a separate experiment (Fig. 9A). Six out of 10 genes were differentially expressed (±1.5-fold change versus control with FDR-adjusted p-value < 0.05), out of which five genes showed the opposite pattern of altered expression in BaP versus DBC-treated mice (Fig. 9B). The five genes were *Birc5*, *Prc1*, *Fech*, *Nqo1*, and *Cyp1b1*.

Overview of altered gene expression in the bone marrow detected by RNA-Seq

Genomic responses were evaluated in bone marrow 24 h post-exposure by RNA-Seq. DBC exposure affected the expression of 4, 94, and 893 genes in the bone marrow (FRD p-value < 0.05; fold change > ± 1.5) at low, medium, and high doses, respectively (Supplementary Table 4). Table 6 provides a comparison between the bone marrow and spleen results for the 10 genes validated by microarrays, RNA-Seq, and RT-PCR. The most striking difference is the strong dose-response and large fold changes in *Cdkn1a* expression in the bone marrow, with 6.3-, 10.6-, and 22.8-fold increases over controls at the low, medium, and high doses, respectively (Table 6). *Cdkn1a* and another gene in the p53 signalling pathway, *Ccnd1*, were two out of only four genes perturbed by DBC at the lowest dose in the bone marrow (Supplementary Table 4).

Consistent with this result, IPA identified p53 activation at medium and high doses in bone marrow RNA-seq profiles, with 13 and 69 differentially expressed genes that are known to be controlled by p53. Out of the 10 genes that were differentially expressed by microarrays, RT-PCR, or both, six genes were also differentially expressed in the bone marrow, as measured by RNA-seq (*Cdkn1a*, *Bbc3*, *Prc1*, *Mtfr1*, *Hmox1,* and *Cyp1b1*) (Table 6). Direction of fold change (i.e, up- or down-regulation) was also consistent between the two tissues. Unlike in the spleen, *Bnip3l* was unaffected in the bone marrow. Overall, genomic responses to the high dose of DBC in the spleen and the bone marrow were very similar. For example, pathway analysis revealed

that five out of the seven top canonical pathways with z-scores above 2.0 were similarly affected by DBC in spleen and bone marrow (Supplementary Fig. 5). In addition, the profiles supported the activation of p53 and Bnip3l in both tissues (Supplementary Table 5).

Benchmark dose (BMD) analysis of toxicogenomics data

In order to achieve our objective of investigating the utility of toxicogenomics for quantitative health risk assessment of immunotoxic compounds, BMD modeling was applied. Table 7 summarizes benchmark dose (BMD) values derived from microarray results. The BMD (BMDL) values ranged from 0.066 (0.025) mg/kg-bw per day for "Heparan sulfate biosynthesis" to 4.46 (2.78) mg/kg-bw per day for the "Cell cycle: G2/M DNA damage checkpoint regulation" pathway. Published literature and our data suggest that DBC exposure affects cell cycle-related pathways, which may be relevant to its immunotoxicity. In addition, AHR signalling is important in mediating many adverse effects associated with PAH exposure. That, along with the fact that "cell cycle: G2/M DNA damage checkpoint regulation", "cyclins and cell cycle regulation" and "aryl hydrocarbon receptor signalling" were the only three IPA pathways that met the default z-score cut-off of 2.0 (Table 2), led us to focus on these IPA pathways of potential relevance to health risk assessment of DBC. We also included the "cellular growth and proliferation, hematological system development & function, hematopoiesis" network containing 11 out of 18 genes that were affected by DBC at all doses. It has previously been suggested that the most sensitive (i.e., with the lowest median BMD values from toxicogenomic data) pathway that contains at least five genes be considered for quantitative risk assessment (e.g., point of departure selection), regardless of its biological significance (Thomas *et al.,* 2011). Thus, we also present the BMD values for the IPA pathway with the lowest BMDLs at the 10^{th} percentile of all affected genes in the network. At 4 h and 24 h, these are "Calcium signaling" and "Heparan

sulfate biosynthesis" with BMD (BMDL) values of 2.2 (0.25) and 0.066 (0.025) mg/kg-bw per day, respectively. In addition, modeling the expression of *Cdkn1a*, a proposed marker of DNA damage response (Li *et al.,* 2015), yielded BMD and BMDL values of 1.7 and 1.2 mg/kg-bw per day, respectively, 4 h post-exposure, using microarray data. Similarly, BMD modeling of RT-PCR data gave BMD and BMDL values of 0.70 and 0.22 mg/kg-bw per day, respectively, 4 h post-exposure. These values are within the range of the pathway BMDs presented in Table 7.

Comparison of toxicogenomic and apical data

Finally, to compare toxicogenomics and traditional toxicity (apical) data, BMD values of potential use in health risk assessment that would be derived from our toxicogenomics and apical (spleen weight) data were compared. The lowest BMDL for toxicogenomic data was for the heparan sulfate biosynthesis pathway (HSBP). In addition to having the lowest BMDL across all pathways, HSBP contained eight genes that could be modelled and had a BMD/BMDL ratio of 2.6 (see Supplementary File 1), indicative of an acceptable fit for the BMD modeling (Moffat *et al.,* 2015). The BMDL for this pathway was 0.025 mg/kg-bw per day. Interestingly, heparan sulfate controls fibroblast growth factor signalling and thus plays a role in controlling stem and progenitor cell fate (reviewed in (Cool and Nurcombe, 2006)-), which is in agreement with our finding that cell cycle-related processes are important for DBC-mediated spleen atrophy. The BMDL values for HSBP and spleen weight (0.025 and 0.095 mg/kg-bw per day, respectively) differed by 3.8. Similarly, the BMDL value for "cellular growth and proliferation, hematological system development & function, hematopoiesis" was 0.080 mg/kg-bw per day, also very much in-line with our apical BMDL.

DISCUSSION

DBC is the most potent carcinogenic PAH studied to date, based on a much higher number of tumors observed in SENCAR female mice in an initiation-promotion study (Higginbotham *et al.*, 1993) and a much larger response in a forward *in vitro* mutation assay (Durant *et al.*, 1996) relative to other PAHs. The present study delves into the immunotoxic effects of DBC, manifested as spleen atrophy in exposed mice, and demonstrates that DBC is genotoxic to both spleen and bone marrow cells. Transcriptional profiling under conditions of induced spleen atrophy and enlargement that take place in mice in response to DBC exposure confirms the importance of p53 signalling, *Cyp1b1* expression, and cell cycle-related pathways. Moreover, the analyses suggest that *Bnip3l* is one of the principal mediators of DBC-induced spleen atrophy. This toxicogenomics study also provides other mechanistic insight into DBC-mediated immunotoxicity. Importantly, the work supports that BMD values produced from pathway analysis are in concordance with apical data. The results generate additional hypotheses, such as the potential involvement of the heparan biosynthesis pathway that is known to regulate growth factor-mediated determination of stem and progenitor cell fate, in the immune-related effects of PAHs. Overall, the pathway perturbations identified in response to DBC are in excellent agreement with its known and emerging genotoxic mode of action, and provide sound explanations for DBC/PAH-mediated immunotoxicity.

The genotoxic effects of DBC on bone marrow are more pronounced than on the spleen as judged by the higher *lacZ* mutant frequency (Fig. 4) and the significant decline in RETs. At the same time, DNA adducts were markedly lower in the bone marrow following DBC exposure, and significantly decreased from 24-h to 72-h (Fig. 3), presumably due to apoptotic removal of bone marrow cells. The observed differences in the frequency of adducts and mutations is

determined by the dynamic interplay between a number of variables that can contribute to these differences, including rates of phase I and II metabolism, DNA damage response and DNA repair pathways, and cell turnover. Toxicogenomics data allow us to explore the reasons for potential differences in adduct and mutant frequencies in the two tissues. The most striking difference observed in our data was the strong dose-response and large fold changes in *Cdkn1a* expression in the bone marrow, with 6.3-, 10.6-, and 22.8-fold increases over controls at the low, medium, and high doses, respectively (Table 6). *Cdkn1a* and another gene in the p53 signalling pathway, *Ccnd1*, were two out of only four genes perturbed by DBC at the lowest dose in the bone marrow (Supplementary Table 4). *Cdkn1a* is upregulated by xenobiotics such as BaP (e.g., (Moffat *et al.,* 2015)) through p53 activation, and plays a role in DNA damage response by inducing cell cycle arrest, inhibition of DNA replication, and apoptosis (reviewed in (Cazzalini *et al.,* 2010)). Cdkn1a can induce cell cycle arrest by several mechanisms, including inhibition of the activity of cyclins involved in the G1, G2, and S-phases of the cell cycle (reviewed in (Cazzalini *et al.,* 2010)). Therefore, greater *Cdkn1a* induction appears to reflect greater sensitivity of the bone marrow over the spleen to DBC exposure.

The percent of MN-RETs in the peripheral blood supports the high degree of genotoxicity historically observed in the bone marrow (US Department of Health and Human Sciences, 2014); the high % MN-RET (Fig. 5) suggests that the bone marrow is a sensitive target of DBC-induced genetic toxicity in mice. Indeed, the % MN-RET was over 4.0 % for the medium dose, which is over 10-fold higher than the maximal range (0.05 – 0.3%) of basal MN-RET levels in most rat and mice strains (reviewed in (Dertinger *et al.,* 2004)) and is thus indicative of a very high genotoxic potency that is rarely achieved by chemical exposure (Dertinger, personal communications). In addition, the % MN-RET observed here at the medium dose of DBC (6.3

mg/kg/day) was four times higher than the % MN-RET induced by a more than 10-fold higher (75 mg/kg/day) dose of BaP in our previous study over 28 days (Lemieux *et al.*, 2011). This very high % MN-RET frequency confirms the much higher mutagenic potency of DBC compared to other PAHs. Similarly, *lacZ* mutant frequency at the high dose of DBC was approximately 2-, 4-, and 8-fold higher in the bone marrow than in the glandular stomach, lung, and liver, respectively, in response to 28-day exposure to a similar dose of 25 mg BaP/kg-bw per day for 28 days (Lemieux *et al.*, 2011,Malik *et al.*, 2012,Labib *et al.*, 2012). These data further support strong mutagenic potency of DBC.

In contrast to other genotoxicity endpoints measured here (i.e., DNA adducts, *lacZ* mutant frequency, and micronuclei formation), 8-oxo-dG levels were increased at the high dose 4 h post-exposure (1.9-fold increase vs. control, Fig. 6) and not 24 h after the last exposure. The results indicate that DBC-mediated DNA oxidation is rapidly repaired in the spleen. This, along with the lack of clear induction of genes related to oxidative stress response, suggests that oxidative stress in the spleen is a secondary effect of DBC exposure and is not directly related to spleen atrophy.

An interesting result in the present study is the central role of Bnip3l in the spleen following DBC exposure. Expression profiles of the spleens of mice exposed to DBC were negatively correlated with those of *Bnip3l* knock-out mice; these two mouse models also exhibit opposing effects on spleen size. Bnip3l is a pro-apoptotic protein that is involved in negative regulation of erythroid maturation. Splenomegaly reported in the *Bnip3l*-deficient mice is associated with erythroblast hyperplasia and reduced apoptosis during erythrocyte maturation (Diwan *et al.*, 2007). It is thus conceivable that erythroid hyperplasia and apoptosis of erythroblasts can directly affect the spleen size (G. W. Dorn II, personal communication). Such a rapid effect on the spleen phenotype seen in response to DBC in our study is consistent with rapid turnover of certain

splenocytes in the mouse, such as dendritic cells that have a half-life of 1.5-2.9 days (Kamath *et al.*, 2000). Splenic *Bnip3l* was down-regulated by DBC at all doses. Therefore, p53-mediated cell cycle arrest and apoptosis of the splenocytes in Muta^{TM}Mouse, and the involvement of Bnip3l in response to DBC, offers a reasonable explanation for the observed spleen atrophy.

The role of Bnip3l and p53-mediated effects on cell cycle and apoptosis in splenocytes in response to DBC, described here, is in accord with previous reports describing marked reduction in the number of spleen and bone marrow cells in response to PAHs. For example, a 5-day exposure of female B6C3F1 mice to BaP resulted in an approximate 2-fold reduction in spleen cellularity (nucleated cells) and bone marrow cellularity ($CD45R^+$ cells) (Holladay and Smith, 1995). Decreased spleen cellularity following BaP exposure was attributed to the effects of BaP on B lymphocyte hematopoiesis in the bone marrow (Holladay and Smith, 1995). Similarly, BaP-mediated splenomegaly in NZB/WF1 mice was characterized by decreased numbers of B (Ig-positive) cells, in parallel with ~2-3-fold increases in the number of null cells (non-T, non-B cells) that are thought to be red blood cell precursors that expand during extramedullary hematopoiesis in the spleen (Booker and White, 2005). Extramedullary hematopoiesis is a compensatory response to hemolysis and may be induced if hematopoiesis in the bone marrow fails to keep up with the replacement needs to maintain adequate circulating levels of red blood cells (reviewed in (Meek *et al.*, 2014)). In addition, damaged erythrocytes are trapped in the mononuclear phagocytic system in the spleen, which also leads to splenomegaly (reviewed in (Petroianu, 2007)). That DBC administration leads to hemolytic anemia is supported by the sharp decrease in reticulocytes observed at all doses (Fig. 5B).

As described above, spleen weight is an important toxicological endpoint, related to the function of the immune system and thus is measured, according to the OECD guideline TG407

(OECD, 2008). However, an important limitation is that although we measured red blood cell count, our study lacked anchoring against other immune function endpoints, such as an assessment using the plaque-forming cell assay. In addition to spleen atrophy, several studies have reported increased spleen weights in laboratory animals in response to PAHs. For example, 30-day exposure of female NZB/WF1 mice to comparable doses of BaP (20 and 40 mg/kg-bw per day) led to ~2-4 fold increases in the spleen weight (Booker and White, 2005). In addition, spleen atrophy followed by splenomegaly has been described in C3H/He mice exposed to single acute doses of cyclophosphamide (Kolb *et al.,* 1977). The response of the spleen to cyclophosphamide in C3H/He mice was characterized by bimodal response of splenocytes (nucleated and Ig-positive cells) consisting of an initial decline (days 0-3 post-exposure), followed by an increase (days 5-9), and a subsequent return to normal levels (days 9-13) (Kolb *et al.,* 1977). Therefore, we hypothesize that spleen atrophy and splenomegaly are the "two sides of the same coin", i.e., we expect that splenomegaly is, at least in part, a compensatory response that arises after spleen atrophy due to increased apoptosis, cell cycle arrest, and hemolytic anemia. More specifically, we hypothesize that both initial atrophy followed by enlargement of the spleen in response to PAHs are mediated by a similar set of genes.

In agreement with our hypotheses, RT-PCR analysis showed the opposite pattern of altered gene expression for five out of 10 genes examined under conditions of enlarged versus atrophied spleens (Fig. 9B). Genes exhibiting opposite expression patterns include the anti-apoptotic proteins Birc5 and Prc1, AHR-regulated Nqo1, CYP1B1, and Fech (the final enzyme in the heme biosynthesis pathway). With respect to AHR regulation of Nqo1 and CYP1B1, it is worth noting that cross talk between AHR and other transcription factors, such as nuclear factor-erythroid 2 p45 subunit-related factor 2 (Nrf2), exists. Indeed, *Nqo1* contains a functional

antioxidant response element and is a subject of transcriptional control of Nrf2 (reviewed in (Moffat *et al.*, 2015)). Down-regulation of the anti-apoptotic genes *Birc5* and *Prc1* following acute exposure to DBC, and up-regulation following subchronic exposure to BaP, is consistent with the notion that activation or inhibition apoptosis in splenocytes and/or their precursors is mechanistically linked to spleen atrophy and enlargement, respectively. *Fech* is transcriptionally up-regulated during low oxygen conditions, presumably to increase heme availability for enhanced erythropoiesis (reviewed in (Chepelev and Willmore, 2011)). Down-regulation of *Fech* during DBC-mediated spleen atrophy is consistent with increased iron availability due to hemolytic anemia. DBC also down-regulated many other genes involved in heme metabolism, including hemoglobin subunit beta-1, hemoglobin alpha, adult chains 1 and 2, erythropoietin receptor, aminolevulinic acid synthase 2, erythroid (Supplementary Table 1). Like Fech, many of these proteins are up-regulated by hypoxia to augment erythropoiesis (reviewed in (Chepelev and Willmore, 2011)). Toxicogenomic profiling of Muta^{TM}Mouse spleen in response to acute administration of DBC suggests increased quantity of reticulocytes and megakaryocytes, inhibited maturation of erythroid cells, inhibited survival of red blood cells, and inhibited survival of erythroid progenitor cells (data not shown). This, in combination with the expression patterns of *Fech*, suggests that heme biosynthesis and hematopoiesis/erythropoiesis are inhibited during PAH-induced spleen atrophy and activated during PAH-induced splenomegaly in mice.

Cyp1b1 was another gene that was altered during spleen atrophy (upregulated) and splenomegaly (downregulated). As described in the introduction, CYP1B1 appears to be important for the metabolic activation of DBC and its immunotoxicity. For example, spleen atrophy in C57BL/6N mice in response to DMBA is abrogated in *Cyp1b1*$^{-/-}$ animals (Gao *et al.*, 2005). In addition, *Cyp1b1* knock-out (in mice) abolishes p53 activation by its phosphorylation

and nuclear translocation in response to DMBA (Gao *et al.*, 2008). It is worth noting that *Cyp1b1* is up-regulated over 160-fold compared to controls 4 h after the last exposure in the lungs of male C57BL/6J mice exposed to 150 mg BaP/kg-bw per day for three days, but then its expression rapidly declines 24 h post-treatment (Moffat *et al.*, 2015), presumably due to the completion of BaP metabolism. Given that 88 days after the last BaP administration in our study all of the BaP is expected to be fully metabolized and eliminated, these persistent changes in *Cyp1b1* expression suggest that it may have other important role(s) in controlling spleen size and, potentially, erythropoiesis that extend beyond xenobiotic metabolism. An important distinction between DBC and BaP that has to be kept in mind while comparing and generalizing the immunotoxic effects of these two compounds is that BaP is metabolized to redox-cycling BaP quinone metabolites that can lead to immunotoxicity through oxidative stress-related pathways (reviewed in (Gao and Burchiel, 2014)). For DBC, on the other hand, oxidative stress appears to only have a minor contribution based on our gene expression data and DNA oxidation measurements.

According to our hypothesis that altered spleen weight is due to perturbations in the same network of genes, *Bnip3l* down-regulation following DBC exposure appears to be an upstream event launched to augment erythropoiesis. As a result, at later time points following DBC exposure splenomegaly may take place, as seen in our case 88 days following 28-day BaP exposure (Fig. 9A). Prolonged downregulation of Bnip3l and, possibly, other pro-apoptotic/tumor suppressor(s) lead(s) to a phenotype that is similar to one described in *Bnip3l*-deficient mice (Diwan *et al.*, 2007). That, in combination with increased steady-state levels of both normal and damaged erythrocytes stored in the spleen, and extramedullary hematopoiesis,

appears as a reasonable mechanism behind increased spleen mass following sub-chronic exposure.

Bnip3l and the other 10 genes that were perturbed by DBC at all doses are part of a "cellular growth and proliferation, hematological system development & function, hematopoiesis" IPA network. That this network is affected by DBC in association with spleen atrophy is not surprising, as the spleen is a major hematopoietic organ in mice. Thus, we argue that the mechanism of action of DBC on the spleen involves perturbations in this pathway leading to toxicity in bone marrow cells, spleen atrophy, and immunotoxicity. The BMDL for this network is 0.080 mg/kg-bw per day, which is comparable to the lowest BMDL for spleen weight (0.095 mg/kg-bw per day) in our study. BMD modeling of the data generated by two different technologies, microarrays and RT-PCR, resulted in very similar BMD values (i.e., BMD(L)s of 1.7(1.2) and 0.70(0.22) mg/kg-bw per day, respectively), using *Cdkn1a*. Increased expression of *Cdkn1a* supports initiation of a DNA damage response (Li *et al.,* 2015). These BMD values are very close to those of the pathways relevant to the immunotoxic MOA of DBC. We previously proposed that toxicogenomics-derived BMDLs can be used in quantitative risk assessment when apical data are not available (Moffat *et al.,* 2015,Chepelev *et al.,* 2015b). The current example with DBC further confirms this notion. Similarly, BMDL values of 0.204 and 0.025 mg/kg-bw per day were found for AHR signalling and heparan sulfate biosynthesis pathways, respectively (Table 8); these BMDLs are also close to the apical BMDL for spleen weight (0.095 mg/kg-bw per day). Thus, our experiment supports the utility of quantitative toxicogenomics for risk assessment of immnotoxic chemicals that are also genotoxic.

More studies are required to determine whether PAHs other than DBC and BaP are immunotoxic in the mouse and, if so, whether that effect involves a similar network of genes.

Our proposed working model for the short- and long-term consequences of PAH exposure, whereby genotoxic stimuli lead to immunotoxicity in the mouse spleen is summarized in Fig. 10. Acute exposure to PAH leads to DNA damage, p53-mediated cell cycle arrest and apoptosis, and hemolytic anemia. Accumulation of damaged erythrocytes in the red pulp of the spleen, as well down-regulation of the pro-apoptotic protein *Bnip3l*, and activation of anti-apoptotic proteins Birc5 and Prc1, as part of a compensatory response to red blood cell loss, are hypothesized to lead to increased erythropoiesis, and extramedullary hematopoiesis in the spleen, thus contributing to splenomegaly. Other hypotheses such as the potential involvement of heparan-mediated regulation of the control of stem and progenitor cell fate of the splenocytes by growth factors are also suggested by the toxicogenomic data. In addition, we highlighted important roles for CYP1B1 and Bnip3l in spleen atrophy and splenomegaly, which can be explored further to determine if/how they are responsible for long-lasting compensatory responses to spleen atrophy, leading to splenomegaly even months after PAH exposure as seen here with BaP. Finally, we demonstrate the utility of toxicogenomics in quantitative health risk assessment of immnotoxic/genotoxic chemicals.

SUPPLEMENTARY DATA

This article is accompanied by five supplementary figures, five supplementary tables, and one supplementary file.

FUNDING

This work was supported by Health Canada's Chemicals Management Plan and the Genomics Research and Development Initiative. Work at King's College London is also supported by Cancer Research UK (Grant C313/A14329).

ACKNOWLEDGEMENTS

We are grateful to Mr. Marc Beal and Dr. Francesco Marchetti for providing us with spleens from the BaP-treated animals.

FIGURE LEGENDS

FIG. 1. Schematic of DBC metabolic activation leading to the ultimate genotoxic carcinogen DBC-11,12-diol-13,14-epoxide and potential mechanism of its immunotoxicity. Structures are redrawn from (Harper *et al.*, 2015). DBC needs to be metabolically activated in order to become a carcinogen; this is primarily carried out by cytochrome P450 (CYP1B1). In addition, DBC activation and resulting immunotoxicity is mediated by microsomal epoxide hydrolase (mEH) (reviewed in (Gao and Burchiel, 2014)). DNA damage-mediated p53 induction may result in transcriptional modulation of the genes involved in DNA repair, apoptosis, and cell cycle arrest, whose function is important for the immune system.

FIG. 2. DBC induces spleen atrophy in Muta™Mouse males. Animals were treated with DBC for 3 consecutive days and spleen weight was determined 4, 24, or 72 h after the last exposure. Shown are means ± standard error of the mean of five animals (A) and representative pictures of spleens for the high dose 72 h post-treatment (B). Differences from controls are indicated as * and ** ($p < 0.05$ and $p < 0.001$, respectively).

FIG. 3. Time- and dose-dependent formation of DBC-DNA adducts in the spleen (A) or bone marrow (B) of Muta™Mouse males treated with DBC and measured 4, 24, and 72 h post-exposure. Error bars represent standard error of the mean of four to five mice (each DNA sample was analyzed in two independent ^{32}P-postlabeling assays). ND, not detected. Differences from controls are indicated as *** ($p < 0.0001$).

FIG. 4. *LacZ* mutant frequency in the spleen and bone marrow of Muta™Mouse males dosed with DBC and measured at 72 h post-exposure. Error bars represent standard error of the mean of five mice. Differences from controls are indicated as ** and *** ($p < 0.001$ and $p < 0.0001$, respectively).

FIG. 5. Frequency of micronucleated reticulocytes (% MN-RET) and micronucleated normochromatic erythrocytes (% MN-NCE) (A) and % reticulocytes (B) in DBC-exposed Muta™ Mouse males. Error bars represent the standard error of the mean of measurement from five animals. Differences from controls are indicated as * and *** ($p < 0.05$ and $p < 0.0001$, respectively).

FIG. 6. Detection of the DNA oxidation marker 8-oxo-dG in the spleens of DBC-exposed Muta™ Mouse males. Error bars represent the standard error of the mean of measurement from four or five separate animals. Difference from the control is indicated as * ($p < 0.05$).

FIG. 7. Negative correlation between spleen profiles of DBC-induced spleen atrophy and splenomegaly in mouse due to *Bnip3l* knock-out. NextBio identified a significant overlap and negative correlation between gene expression changes in the spleens of DBC exposed mice relative to controls (Bioset 1: our study) and gene expression changes in the spleens of *Bnip3l*-(aka *Nix*) deficient mice compared to wildtype from (Diwan *et al.*, 2007) (Bioset 2).

FIG. 8. Confirmation of Bnip3l downregulation in DBC-exposed Muta™Mouse spleen by immunoblotting. Differences from the controls are indicated as * ($p < 0.05$, n=3).

FIG. 9. Identification of genes involved in mediating spleen atrophy and enlargement in the Muta™Mouse model in response to PAH exposure. A. Alterations in spleen weight as a result of BaP exposure (daily to 100 mg/kg-bw, for 28 days, measured 88 days after the last exposure). B.

The expression of 10 genes in both spleen atrophy and enlargement models that are hypothesized to belong to the same gene network that determines alterations of the spleen size in response to PAH exposure. Differences from the controls are indicated as * ($p < 0.05$, n=3-5).

FIG. 10. Working model of PAH-induced alterations in spleen size. Under normal homeostatic conditions (A), differentiation of hematopoietic progenitor cells into erythrocytes is determined by a balance between pro-apoptotic (e.g., Bnip3l) and cell growth and proliferation pathways. Genotoxic compounds like DBC and other PAHs activate p53-mediated apoptosis and inhibit cell proliferation, leading to reticulocyte (Fig. 4B) and splenocyte loss (measured indirectly as spleen atrophy (Fig.1) (B). Prolonged downregulation of Bnip3l and, possibly, other pro-apoptotic/tumor suppressors leads to the phenotype, similar to one described in *Bnip3l*-defficient mouse (Diwan *et al.,* 2007). That, in combination with increased steady-state levels of both normal and damaged erythrocytes that are stored in the spleen, and extramedullary hematopoiesis, leads to increased spleen mass following sub-chronic exposure (C).

SUPPLEMENTARY FIGURE LEGENDS

Supplementary Fig. 1. Lack of dose-dependent effects of DBC exposure on the liver weight in the Muta™Mouse model. * denotes statistically-significant differences from controls ($p < 0.05$).

Supplementary Fig. 2. Representative autoradiographic profiles of DBC-DNA adducts detected by ^{32}P-postlabeling in the spleen and bone marrow of the Muta™Mouse exposed to DBC. The origin, at the bottom left-hand corner, was cut off before imaging.

Supplementary Fig. 3. Hierarchical cluster analysis of the DBC-induced alteration in gene expression in the spleen of the Muta™Mouse detected by Agilent DNA microarrays 4 or 24 h

after the last exposure. D0, D1, D2, and D3 indicate control, low, medium, and high doses; T1 and T2 stand for 4 or 24 h post-exposure; horizontal rows are genes and vertical rows are conditions. Animal numbers were added to designate each sample, such that e.g. D3T2_34 stands for high dose, 24h post-exposure, animal number 34.

Supplementary Fig. 4. Concordance between DNA microarrays and RNA-Sequencing profiling of gene expression in the spleens of Muta™Mouse following DBC exposure.

Supplementary Fig. 5. Top pathways affected by DBC in the bone marrow and spleen of Muta™Mouse are related to cell cycle and aryl hydrocarbon signalling.

SUPPLEMENTARY FILE LEGEND

Supplementary File 1. Benchmark dose (BMD) values derived from toxicogenomics data at the 10th percentile of all affected genes in the spleen of Muta™Mouse 4 or 24 h after the last exposure to DBC for each canonical pathway, containing at least 5 genes that can be modelled and with BMD/BMDL < 10.

SUPPLEMENTARY TABLES

Supplementary Table 1. Agilent probes affected by the low, medium, and high doses of DBC in the spleens of Muta ™Mouse males 4 h and 24 h after the last treatment. Probes presented had false discovery rate- (FDR)-adjusted p-value < 0.05 and fold change ≥ 1.5 in at least one dose and time point (see Gene Expression Omnibus, accession number GSE72334, for all probes).

Supplementary Table 2. Upstream regulators identified by Ingenuity Pathway Analysis (z-score§ ≥ ±2.0) in the spleens of Muta™Mouse males dosed with DBC.

Supplementary Table 3. Differentially expressed genes (false discovery rate- (FDR)-adjusted p-value < 0.05, fold change ≥ 1.5 relative to controls) as identified by RNA-Seq in spleens 4 h after the last exposure of Muta^{TM}Mouse males to 20.0 mg DBC/kg bw per day.

Supplementary Table 4. Differentially expressed genes (false discovery rate- (FDR)-adjusted p-value < 0.05, fold change ≥ 1.5 relative to controls) in bone marrow 24 h after the last exposure of Muta^{TM}Mouse males to DBC.

Supplementary Table 5. Upstream regulators identified by Ingenuity Pathway Analysis (z-score§ ≥ 2.0) in the bone marrow of Muta^{TM}Mouse males exposed to DBC.

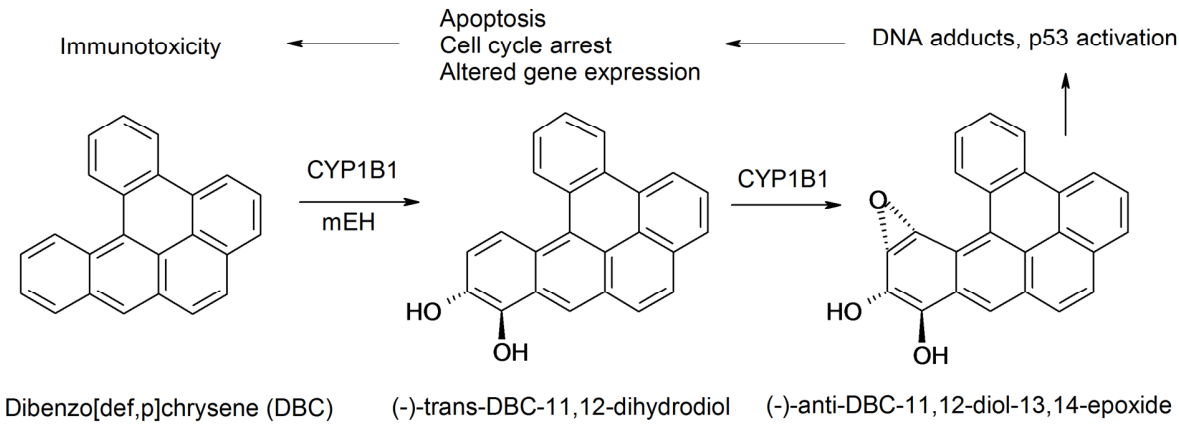
Immunotoxicity
Apoptosis
Cell cycle arrest
Altered gene expression
DNA adducts, p53 activation
CYP1B1
mEH
CYP1B1
HO
OH
O
HO
OH
Dibenzo[def,p]chrysene (DBC)
(-)-trans-DBC-11,12-dihydrodiol
(-)-anti-DBC-11,12-diol-13,14-epoxide

FIG. 1.

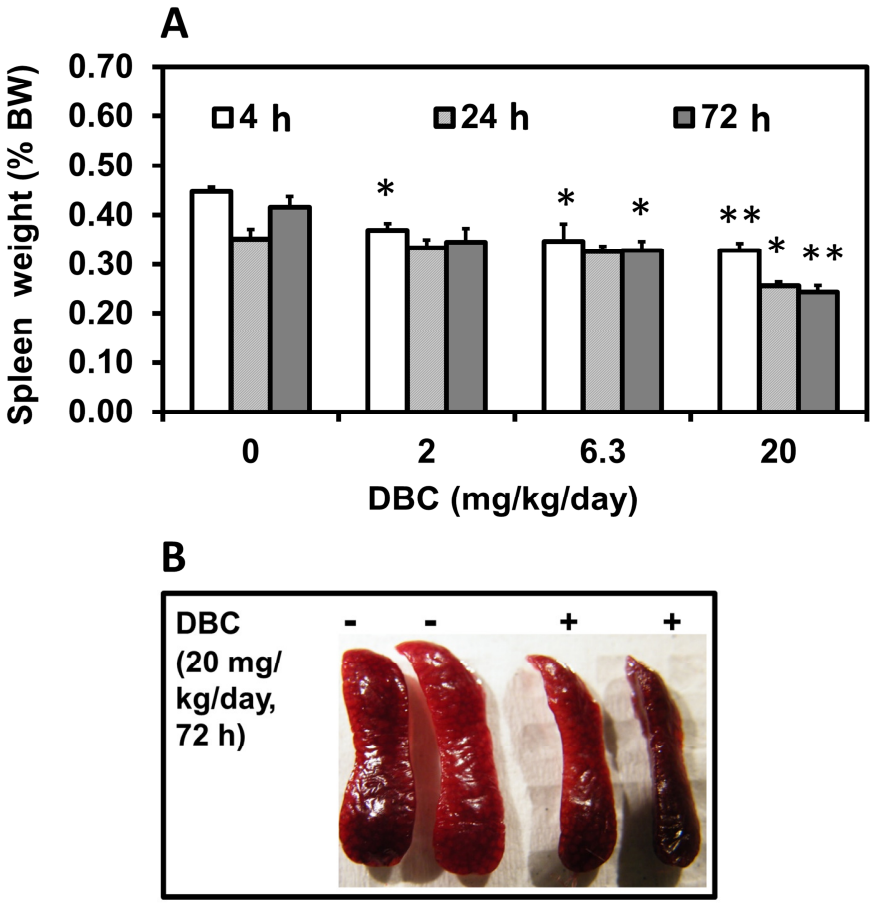
A
Spleen weight (% BW)
0.70
0.60
0.50
0.40
0.30
0.20
0.10
0.00
4 h
24 h
72 h
*
*
*
*
**
*
**
0
2
6.3
20
DBC (mg/kg/day)
B
DBC
(20 mg/
kg/day,
72 h)
-
-
+
+

Figure 2

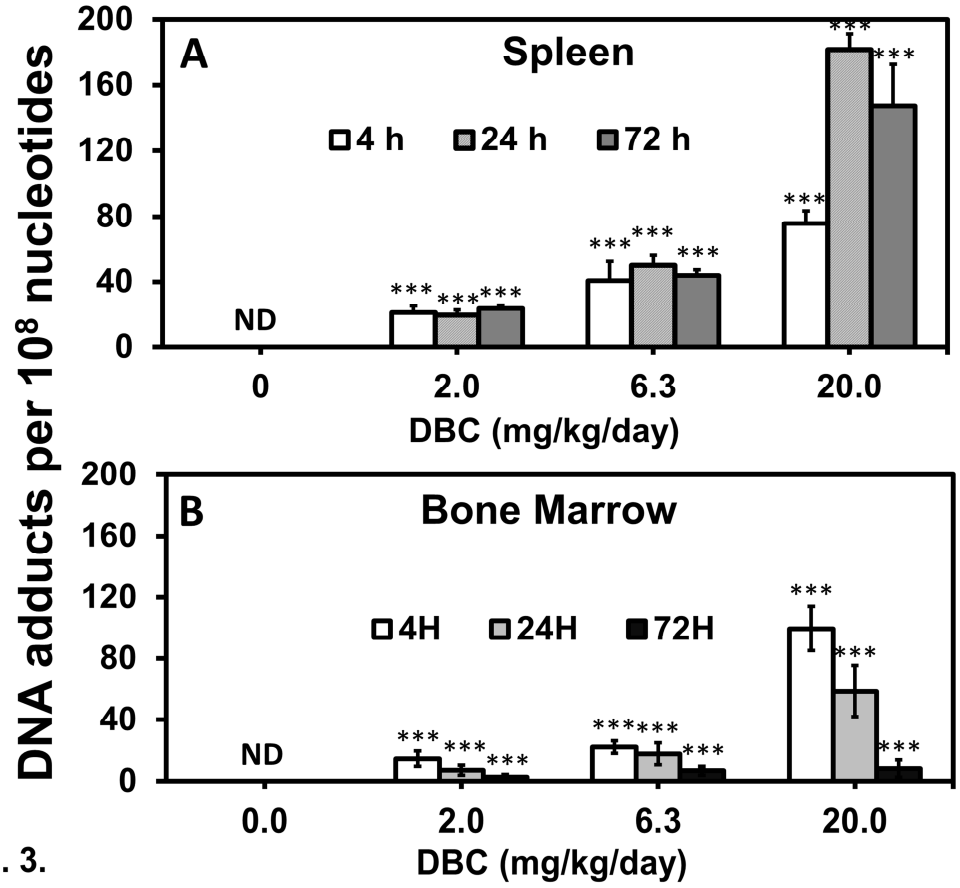

FIG. 3.

Figure 3

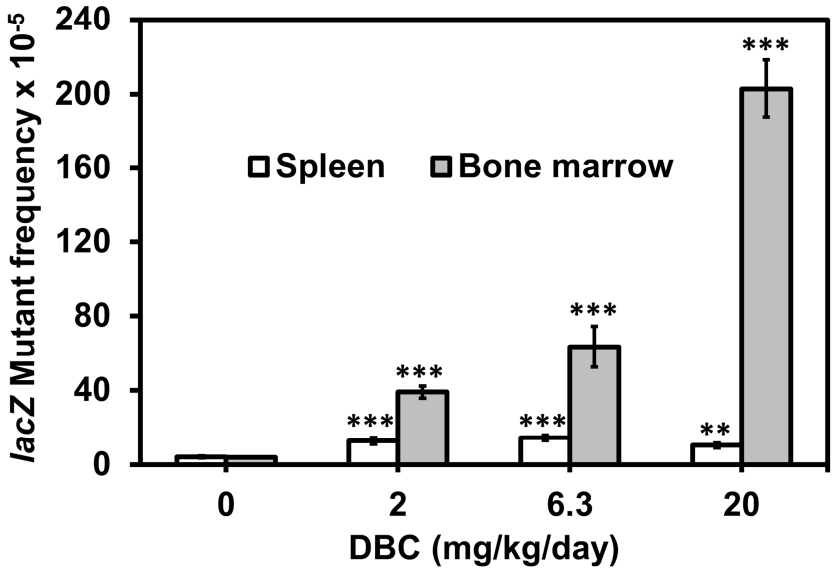

FIG. 4.

Figure 4

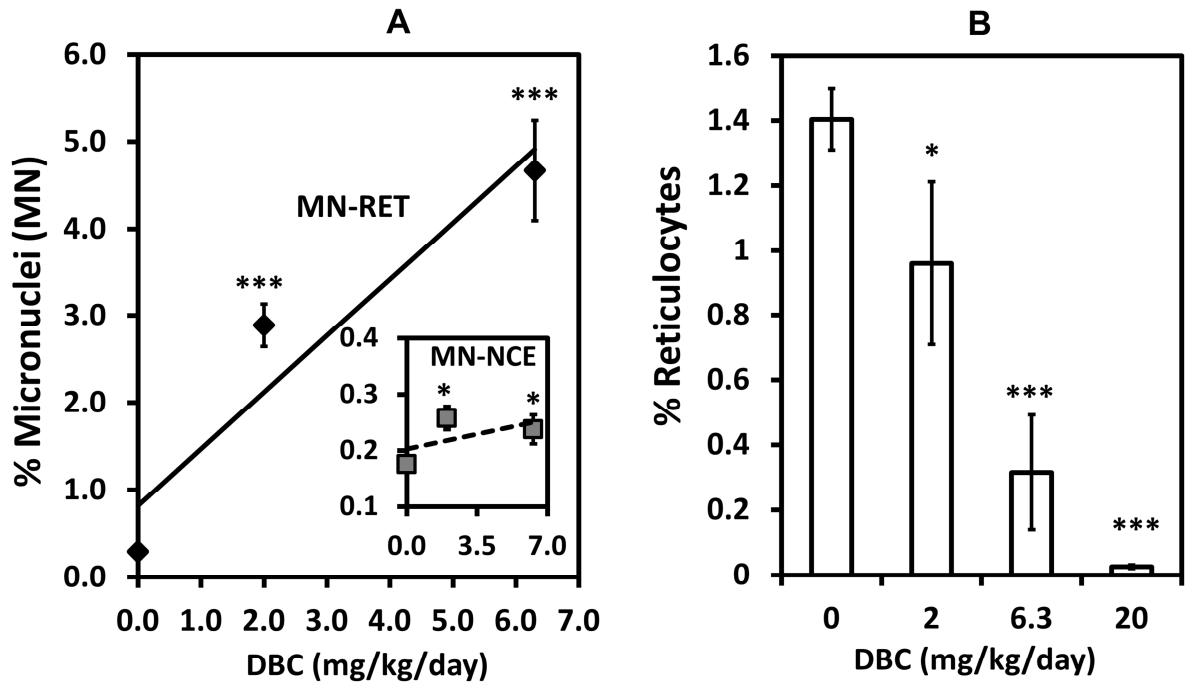

FIG. 5.

Figure 5

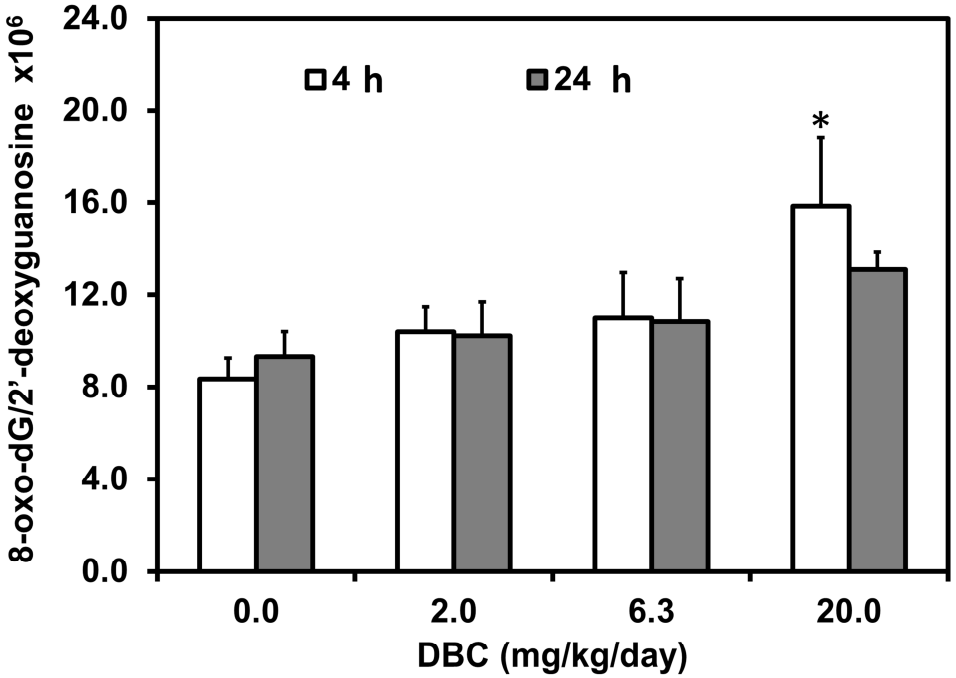

FIG. 6.

Figure 6

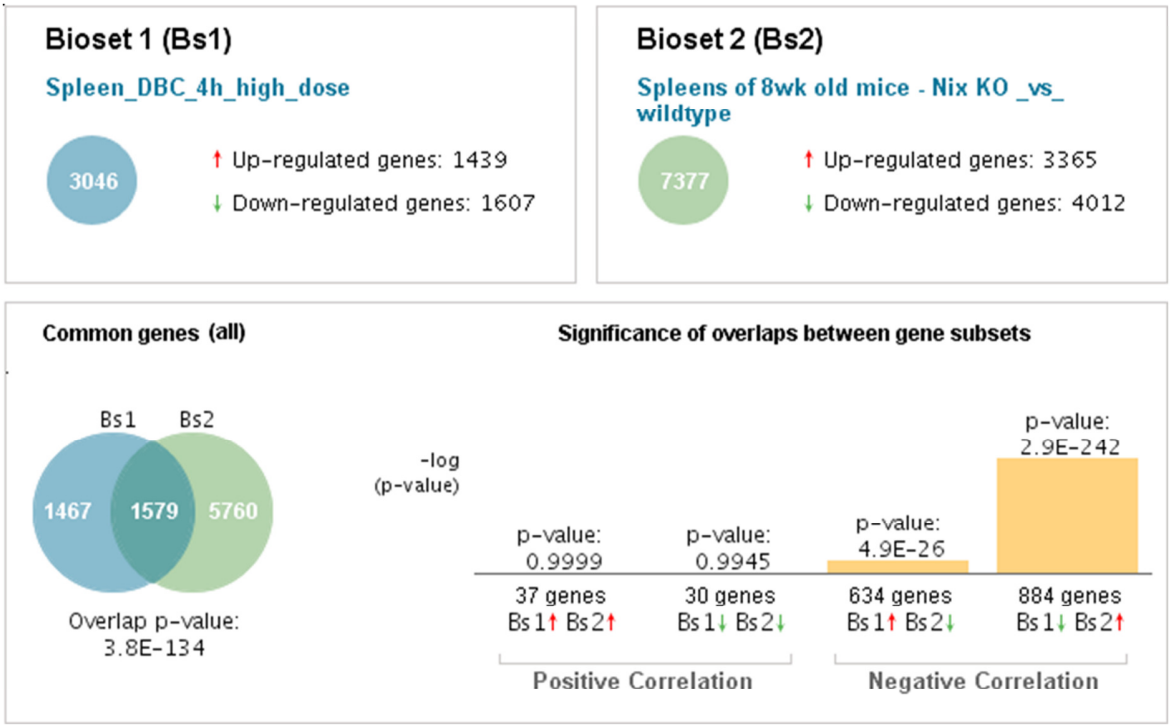

FIG. 7.

Figure 7

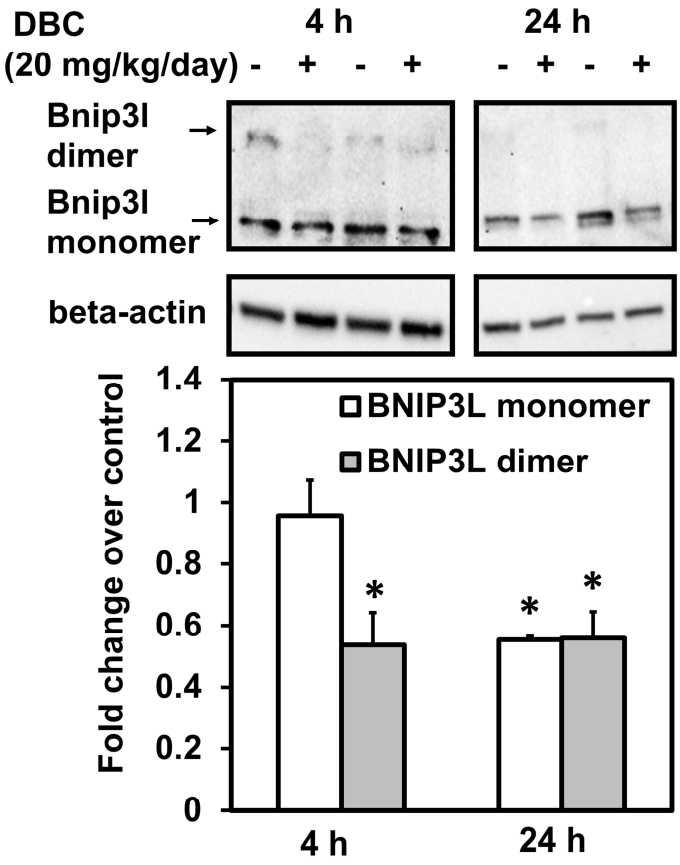

FIG. 8.

Figure 8

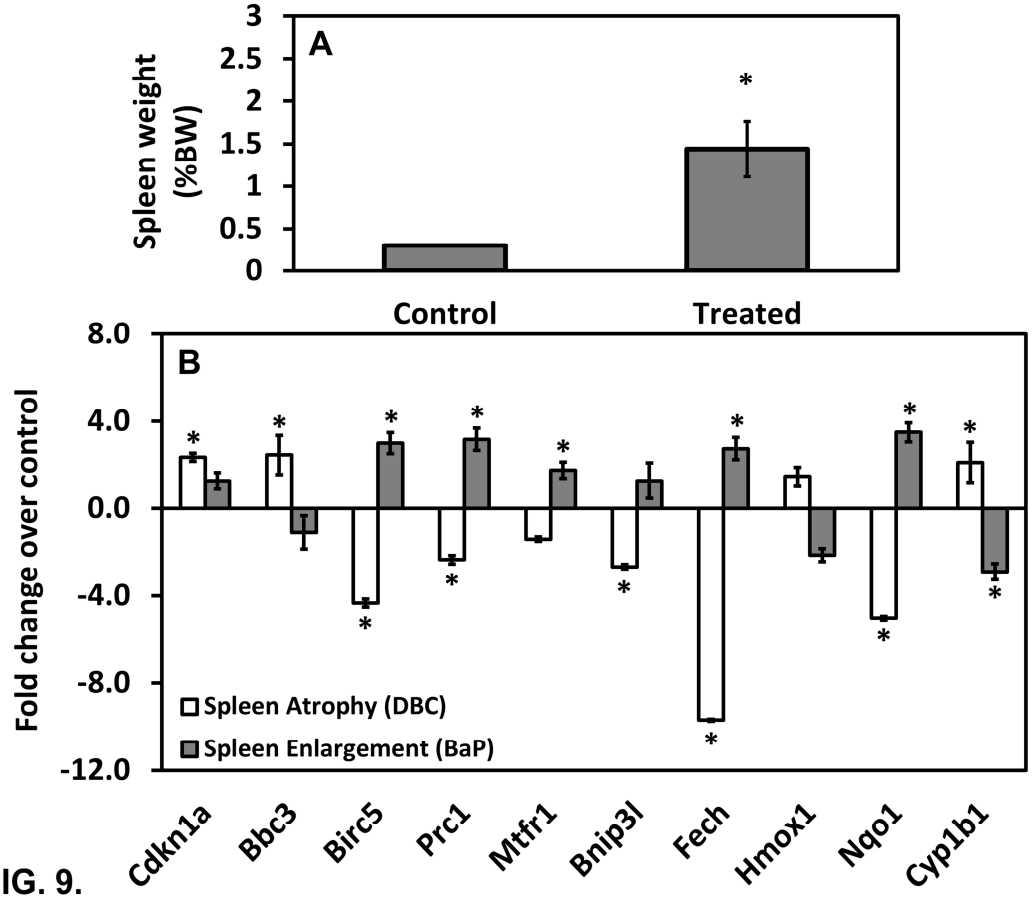

FIG. 9.

Figure 9

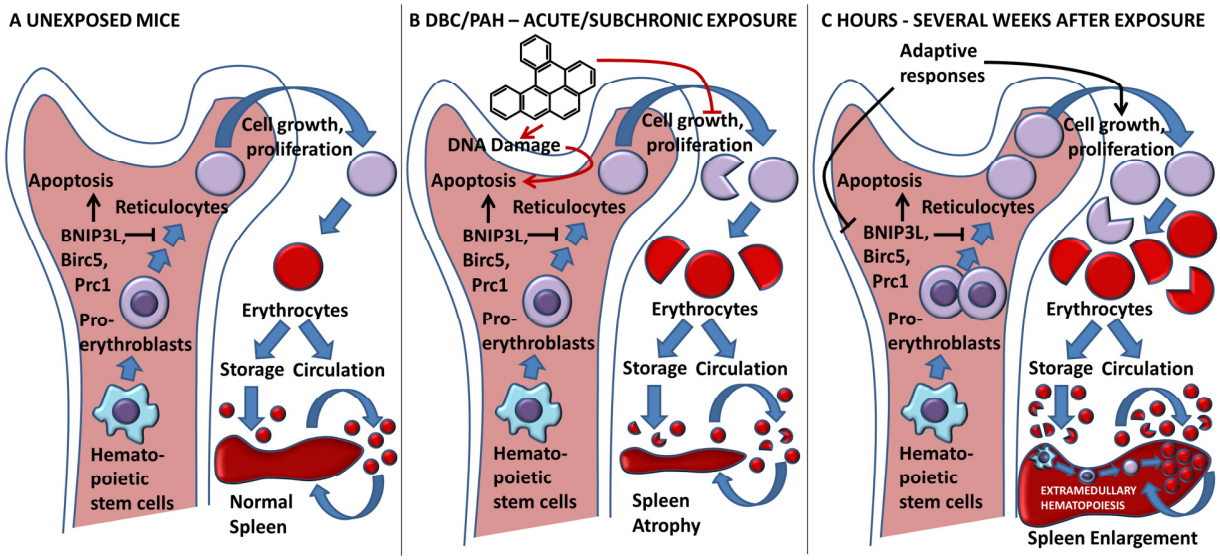
A UNEXPOSED MICE
Cell growth, proliferation
Apoptosis
Reticulocytes
BNIP3L, Birc5, Prc1
Pro-erythroblasts
Hemato-poietic stem cells
Erythrocytes
Storage
Circulation
Normal Spleen
B DBC/PAH – ACUTE/SUBCHRONIC EXPOSURE
DNA Damage
Cell growth, proliferation
Apoptosis
Reticulocytes
BNIP3L, Birc5, Prc1
Pro-erythroblasts
Hemato-poietic stem cells
Erythrocytes
Storage
Circulation
Spleen Atrophy
C HOURS - SEVERAL WEEKS AFTER EXPOSURE
Adaptive responses
Cell growth, proliferation
Apoptosis
Reticulocytes
BNIP3L, Birc5, Prc1
Pro-erythroblasts
Hemato-poietic stem cells
Erythrocytes
Storage
Circulation
EXTRAMEDULLARY HEMATOPOIESIS
Spleen Enlargement

Figure 10

TABLES

TABLE 1. Function of the eighteen genes that were perturbed by all doses of DBC in the spleens of Muta^{TM}Mouse.

Gene name	Entrez gene ID	Entrez gene name	Function (if known)	References
4921504E06Rik	70909	RIKEN cDNA 4921504E06 gene		
BNIP3L	100043324|12177	BCL2/adenovirus E1B 19kDa interacting protein 3-like	Pro-apoptotic protein; promotes apoptosis during erythropoiesis to control red blood cell number and to preferentially eliminate abnormal erythrocytes. Mediates mitochondrial clearance by autophagy (mitophagy) in erythrocytes.	(Diwan *et al.*, 2008,Ding *et al.*, 2010,Zhang *et al.*, 2012)
C20orf144		--		
CCDC42B	546886	Coiled-coil domain containing 42B		
CCNDBP1	17151	Cyclin D-type binding-protein 1	May negatively regulate cell cycle progression by inhibition of the cyclin-D1/CDK4 complex, thereby preventing phosphorylation of RB1 and blocking E2F-dependent transcription.	(Safran *et al.*, 2010)
EPHB6	13848	EPH receptor B6	Transmembrane proteins receptor for ephrin-B family; influences cell adhesion and migration.	(Safran *et al.*, 2010)
FAM220A	67238	Family with sequence similarity 220, member A	Accelerates dephosphorylation of transcription factor STAT3 (signal transducer and activator of transcription 3), inhibiting its activity.	(Ren *et al.*, 2013)
FCHSD1	319262	FCH and double SH3 domains 1	F-actin regulatory protein; development and/or maintenance of the F-actin cytoskeleton.	(Cao *et al.*, 2013)
FGF13	14168	fibroblast growth factor 13	Broad mitogenic and cell survival activities: embryonic development, cell growth, morphogenesis, tissue repair, tumor growth, and invasion.	(Safran *et al.*, 2010)
Gm6792	627821	Predicted gene 6792		
Gm6936	628951	Predicted gene 6936		

TABLE 1. (Continued).

Gm4836 (includes others)		--		
MBD5		--	Regulates iron metabolism by regulating gene expression of ferritin light chain gene (Ftl1; knock out of MBD5 leads to reduced intestinal levels of Ftl1 mRNA).	(Safran *et al.*, 2010,Tao *et al.*, 2014)
NCOA4	27057	Nuclear receptor coactivator 4	Selective cargo receptor for autophagic turnover of ferritin (ferritinophagy); critical for iron homeostasis.	(Mancias *et al.*, 2014)
PPP1CB	19046	Protein phosphatase 1, catalytic subunit, beta isozyme	Protein phosphatase; essential for cell division, regulates glycogen metabolism, muscle contractility and protein synthesis. Iron-binding protein.	(Safran *et al.*, 2010)
SOX13	20668	SRY (sex determining region Y)-box 13	Regulation of embryonic development and in the determination of cell fate.	(Safran *et al.*, 2010)
Stfa3	20863	Stefin A3	Cysteine protease inhibitor; epidermal development and maintenance.	(Safran *et al.*, 2010)
YIPF4	67864	Yip1 domain family, member 4	Maintenance of the Golgi structure.	(Safran *et al.*, 2010)

TABLE 2. Canonical pathways identified by Ingenuity Pathway Analysis as being affected by DBC in the spleens of Muta™Mouse and for which activity prediction z-score[§] is available.

Time point	Dose	Pathway	p-value*	z-score
4 h	low	None		
4 h	med.	None		
4 h	high	Role of BRCA1 in DNA damage response	3.32E-05	-0.6
		Estrogen-mediated S-phase entry	3.64E-05	-1.1
		Cyclins and cell cycle regulation	2.65E-04	-1.4
		Cell cycle: G2/M DNA damage checkpoint regulation	**3.87E-04[#]**	**2.3**
		Cell cycle: G1/S checkpoint regulation	2.01E-03	0.3
		Complement system	4.43E-03	1.3
		Role of CHK proteins in cell cycle checkpoint control	8.01E-03	0.8
		ATM signaling	1.54E-02	-0.4
		Aryl hydrocarbon receptor signaling	1.69E-02	-1.9
24 h	low	None		
24 h	med.	Cell cycle: G2/M DNA damage checkpoint regulation	5.83E-04	1.6
		Cyclins and cell cycle regulation	2.09E-02	-1.3
		Estrogen-mediated S-phase entry	6.64E-05	-1.6
24 h	high	**Cell cycle: G2/M DNA damage checkpoint regulation**	**3.1E-04**	**2.1**
		Role of BRCA1 in DNA damage response	3.8E-04	-0.7
		Cyclins and cell cycle regulation	**4.7E-04**	**-2.1**
		ATM signaling	3.9E-03	-1.1
		Cell cycle: G1/S checkpoint regulation	5.4E-03	1.1
		Aryl hydrocarbon receptor signaling	**1.5E-02**	**-2.1**
		Pancreatic adenocarcinoma signaling	1.7E-02	-1.0
		Role of CHK proteins in cell cycle checkpoint control	2.7E-02	0.4

[§]Z-score assesses the match of observed and predicted up/downregulation patterns; positive z-score indicates activation, negative - inhibition.

*P-value for Fisher's exact test measuring the overlap of observed and predicted regulated gene sets is shown.

[#]Shown in bold are values with z-score > 2.0 (default cut-off for activation or inhibition in IPA).

TABLE 3. Agilent microarray data for the genes selected for RT-PCR-validation in the Muta™Mouse spleen following DBC exposure.

Agilent probe ID	Gene Symbol	*Gene expression 4 h after 3-day gavage*						*Gene expression 24 h after 3-day gavage*					
		2.0 mg/kg-bw		6.3 mg/kg-bw		20.0 mg/kg-bw		2.0 mg/kg-bw		6.3 mg/kg-bw		20.0 mg/kg-bw	
		Fold change	FDR p-value	Fold change	FDR p-value	Fold change	FDR p-value	Fold change	FDR p-value	Fold change	FDR p-value	Fold change	FDR p-value
A_51_P363947	*Cdkn1a*	**1.62**[*]	**0.034**	**1.95**	**0.000**	**1.58**	**0.003**	1.27	0.487	1.40	0.156	1.47	0.006
A_51_P248122	*Bbc3*	1.40	0.228	1.26	0.579	1.44	0.012	1.42	0.047	1.43	0.041	**1.71**	**0.000**
A_55_P1983768	*Birc5*	1.19	0.955	-1.53	0.666	**-4.10**	**0.000**	-1.62	0.418	**-2.28**	**0.027**	**-3.76**	**0.000**
A_55_P1988083	*Prc1*	1.00	0.999	-1.56	0.564	**-3.29**	**0.000**	-1.68	0.207	**-2.08**	**0.011**	**-3.49**	**0.000**
A_52_P575771	*Mtfr1*	1.11	0.955	-1.36	0.521	**-2.12**	**0.000**	-1.30	0.490	-1.55	0.056	**-1.83**	**0.002**
A_55_P1961463	*Bnip3l*	**-1.88**	**0.000**	**-2.64**	**0.000**	**-3.98**	**0.000**	**-1.85**	**0.000**	**-2.25**	**0.000**	**-2.56**	**0.000**
A_55_P2042146	*Fech*	-1.53	0.953	**-4.07**	**0.000**	**-21.60**	**0.000**	**-2.96**	**0.000**	**-5.76**	**0.000**	**-14.08**	**0.000**
A_55_P2029687	*Hmox1*	-1.14	0.953	1.05	0.960	1.19	0.547	-1.11	0.830	-1.03	0.965	**1.59**	**0.014**
A_51_P424338	*Nqo1*	1.02	0.991	-1.28	0.659	**-1.53**	**0.019**	-1.25	0.571	**-1.56**	**0.033**	**-1.51**	**0.012**
A_51_P255456	*Cyp1b1*	1.19	0.953	1.30	0.593	1.44	0.025	1.21	0.625	1.25	0.499	1.48	0.008
A_55_P2186027	*Gapdh*	1.08	0.953	1.18	0.666	1.21	0.169	-1.03	0.916	1.02	0.967	-1.02	0.940

[*]Values above 1.5-fold change and false-discovery rate- (FDR) adjusted p-value < 0.05 are in **bold**.
Gene expression values were normalized to *Gapdh.*

TABLE 4. Validation of microarray results by RT-PCR for selected genes in the Muta™Mouse spleen following DBC exposure

Accession number	Gene Symbol	*Gene expression 4 h after 3-day gavage*						*Gene expression 24 h after 3-day gavage*					
		2.0 mg/kg-bw		6.3 mg/kg-bw		20.0 mg/kg-bw		2.0 mg/kg-bw		6.3 mg/kg-bw		20.0 mg/kg-bw	
		Fold change[§]	FDR p-value	Fold change	FDR p-value	Fold change	FDR p-value	Fold change	FDR p-value	Fold change	FDR p-value	Fold change	FDR p-value
NM_007669	*Cdkn1a*	**2.06**[*]	**0.006**	**2.48**	**0.002**	**2.36**	**0.002**	**2.63**	**0.028**	**3.32**	**0.010**	**2.24**	**0.009**
NM_133234	*Bbc3*	1.54	0.206	1.67	0.072	**2.47**	**0.005**	**1.64**	**0.023**	**1.65**	**0.007**	1.28	0.531
NM_009689	*Birc5*	-1.87	0.341	-1.48	0.1480	**-4.33**	**0.023**	1.50	0.312	-1.53	0.853	**-9.26**	**0.027**
NM_145150	*Prc1*	-1.69	0.097	-1.49	0.084	**-2.34**	**0.018**	1.27	0.386	-1.23	0.889	**-3.26**	**0.035**
NM_026182	*Mtfr1*	-1.31	0.277	-1.03	0.414	-1.40	0.007	1.24	0.199	-1.11	0.855	1.26	0.264
NM_009761	*Bnip3l*	**-2.41**	**0.039**	**-1.60**	**0.019**	**-2.66**	**0.038**	-1.18	0.583	-1.92	0.127	**-3.90**	**0.032**
NM_007998	*Fech*	**-3.30**	**0.008**	**-4.37**	**0.000**	**-9.69**	**0.001**	1.07	0.844	-3.11	0.296	**-22.77**	**0.019**
NM_010442	*Hmox1*	-1.16	0.243	1.05	0.955	1.48	0.955	1.31	0.096	1.20	0.174	1.23	0.434
NM_008706	*Nqo1*	**-2.19**	**0.0009**	**-2.29**	**0.027**	**-5.02**	**0.012**	1.61	0.384	-1.58	0.593	**-7.15**	**0.069**
NM_009994	*Cyp1b1*	1.19	0.494	1.28	0.277	**2.12**	**0.009**	1.32	0.116	1.27	0.211	1.33	0.044

[§]With respect to controls for each time point; values were normalized to glyceraldehyde-3-phosphate dehydrogenase (Gapdh; NM_008084) expression.

[*]Values above 1.5-fold change and false-discovery rate- (FDR) adjusted p-value < 0.05 are in **bold**.

TABLE 5. The expression of selected genes measured by microarrays, RT-PCR, and RNA-Seq in the spleens of Muta^{TM}Mouse 4 h following exposure to 20.0 mg DBC/kg bw per day for three days.

Accession number	Gene Symbol	Microarrays		RT-PCR		RNA-Seq	
		Fold change	FDR p-value	Fold change	FDR p-value	Fold change	FDR p-value
NM_007669	*Cdkn1a*	**1.58**[*]	**0.000**	**2.36**	**0.002**	**2.90**	**0.000**
NM_133234	*Bbc3*	1.44	0.010	**2.47**	**0.005**	**4.00**	**0.000**
NM_009689	*Birc5*	**-1.50**	**0.000**	**-4.33**	**0.023**	**-5.50**	**0.000**
NM_145150	*Prc1*	**-3.29**	**0.000**	**-2.34**	**0.018**	**-6.00**	**0.000**
NM_026182	*Mtfr1*	**-2.12**	**0.000**	-1.40	0.007	**-3.80**	**0.000**
NM_009761	*Bnip3l*	**-3.98**	**0.000**	**-2.66**	**0.038**	**-3.40**	**0.000**
NM_007998	*Fech*	**-21.6**	**0.000**	**-9.69**	**0.001**	**-11.80**	**0.000**
NM_010442	*Hmox1*	1.19	0.550	1.48	0.955	**2.10**	**0.000**
NM_008706	*Nqo1*	**-1.53**	**0.020**	**-5.02**	**0.012**	**-4.90**	**0.000**
NM_009994	*Cyp1b1*	1.44	0.020	**2.12**	**0.009**	-1.04	0.85
NM_008084	*Gapdh*	1.21	0.169	1.00	0.000	1.37	0.227

[*]Values above 1.5-fold change and false-discovery rate- (FDR) adjusted p-value < 0.05 are in **bold**.

TABLE 6. Comparison of the expression of selected genes in the spleen and the bone marrow of Muta™Mouse 24 h following three-day exposure to DBC.

Accession number	Gene Symbol	*Spleen*						*Bone Marrow*					
		2.0 mg/kg-bw		6.3 mg/kg-bw		20.0 mg/kg-bw		2.0 mg/kg-bw		6.3 mg/kg-bw		20.0 mg/kg-bw	
		Fold change	FDR p-value	Fold change	FDR p-value	Fold change	FDR p-value	Fold change	FDR p-value	Fold change	FDR p-value	Fold change	FDR p-value
NM_007669	*Cdkn1a*	1.27	0.487	1.40	0.156	1.47	0.006	**6.27**	**0.000**	**10.63**	**0.000**	**22.78**	**0.000**
NM_133234	*Bbc3*	1.42	0.047	1.43	0.041	**1.71**	**0.000**	1.28	0.858	1.65	0.283	**2.68**	**0.001**
NM_009689	*Birc5*	-1.62	0.418	**-2.28**	**0.027**	**-3.76**	**0.000**	1.10	0.921	-1.04	0.942	-1.45	0.186
NM_145150	*Prc1*	-1.68	0.207	**-2.08**	**0.011**	**-3.49**	**0.000**	1.08	0.933	-1.20	0.590	**-1.72**	**0.019**
NM_026182	*Mtfr1*	-1.30	0.490	-1.55	0.056	**-1.83**	**0.002**	1.17	0.862	-1.19	0.674	**-1.73**	**0.038**
NM_009761	*Bnip3l*	**-1.85**	**0.000**	**-2.25**	**0.000**	**-2.56**	**0.000**	1.12	0.922	1.12	0.846	-1.36	0.388
NM_007998	*Fech*	**-2.96**	**0.000**	**-5.76**	**0.000**	**-14.08**	**0.000**	1.23	0.848	1.04	0.959	-1.35	0.425
NM_010442	*Hmox1*	-1.11	0.830	-1.03	0.965	**1.59**	**0.014**	1.55	0.515	1.56	0.183	**3.20**	**0.000**
NM_008706	*Nqo1*	-1.25	0.571	**-1.56**	**0.033**	**-1.51**	**0.012**	-1.56	0.735	-1.30	0.719	-1.51	0.436
NM_009994	*Cyp1b1*	1.21	0.625	1.25	0.499	1.48	0.008	1.63	0.550	1.45	0.446	**2.95**	**0.000**
NM_008084	*Gapdh*	-1.03	0.916	1.02	0.967	-1.02	0.940	1.03	0.993	1.11	0.874	1.29	0.501

*Values above ± 1.5-fold change and false-discovery rate- (FDR) adjusted p-value < 0.05 are in **bold**.

TABLE 7. Benchmark dose (BMD) values derived from toxicogenomics data at the 10th percentile of all affected genes in the spleen of Muta™Mouse in: (a) each canonical pathway activated or inhibited (z-score ≥ 2.0), (b) network comprising most sensitive (affected at all doses and time points) genes, or (c) most sensitive[¶] pathway

Time post-treatment	Ingenuity Pathway Analysis pathway or network	Number of genes modelled	BMD[*] (mg/kg-bw per day)	BMDL (mg/kg-bw per day)
4 h	Cell cycle: G2/M DNA damage checkpoint regulation (a)	17	4.46	2.78
	Cellular growth and proliferation, hematological system development & function, hematopoiesis network (b)	7	0.71	0.35
	Calcium signaling (c)	45	2.20	0.25
24 h	Cell cycle: G2/M DNA damage checkpoint regulation (a)	13	1.69	0.07
	Cyclins and cell cycle regulation (a)	25	1.07	< 0.02
	Aryl hydrocarbon receptor signaling (a)	37	1.86	**0.20[§]**
	Cellular growth and proliferation, hematological system development & function, hematopoiesis network (b)	15	0.17	**0.080**
	Heparan sulfate biosynthesis (c)	8	0.066	**0.025**

[¶]Similar to (Thomas *et al.*, 2011), but examined lowest BMDLs at the 10th percentile rather than lowest median BMDLs.

[*]BMD and BMDL (lower confidence limit on BMD) were calculated with default benchmark response of one standard deviation.

[§]Lowest BMDL values for each approach (a, b, or c) are in **bold** (provided BMD/BMDL > 10).

Note: BMD(L) values that were less than 1% of the lowest dose administered (i.e., 0.02 mg/kg bw per day) and/or those that produced BMD/BMDL ratio > 10.0 (indicative of poor fit) were not considered.

TABLE 8. Comparison of BMD values derived from toxicogenomis (lowest BMDLs for each of toxicogenomics approach presented in Table 7) and apical (spleen weight) data with potential relevance to health risk assessment of DBC.

Time post-treatment	Most sensitive toxicogenomic endpoints	Transcriptional BMDL (mg/kg-bw per day)	Apical (spleen weight) BMDL (mg/kg-bw per day)
4 h	None (all most sensitive pathways come from 24-hr time point)		**0.095**[¶]
	Aryl hydrocarbon receptor signaling pathway	0.204	
24 h	Cellular growth and proliferation, hematological system development & function, hematopoiesis network	0.080	4.44
	Heparan sulfate biosynthesis pathway	**0.025**[§]	
72 h	None (see above)		0.707

[¶]Corresponding benchmark dose (BMD) value is 0.257 mg/kg-bw per day, making BMD/BMDL ratio equal to 2.7.

[§]BMDL values for toxicogenomics and spleen weight data that are the lowest and thus proposed as PODs for DBC-mediated immunotoxicity are in **bold**.

Note: BMD(L) were calculated with default benchmark response of one standard deviation.

REFERENCES

Booker, C. D. and White, K. L.,Jr. (2005). Benzo(a)pyrene-induced anemia and splenomegaly in NZB/WF1 mice. *Food Chem. Toxicol.* **43,** 1423-1431.

Cao, H., Yin, X., Cao, Y., Jin, Y., Wang, S., Kong, Y., Chen, Y., Gao, J., Heller, S., and Xu, Z. (2013). FCHSD1 and FCHSD2 are expressed in hair cell stereocilia and cuticular plate and regulate actin polymerization in vitro. *PLoS One.* **8,** e56516.

Cazzalini, O., Scovassi, A. I., Savio, M., Stivala, L. A., and Prosperi, E. (2010). Multiple roles of the cell cycle inhibitor p21(CDKN1A) in the DNA damage response. *Mutat. Res.* **704,** 12-20.

Cesta, M. F. (2006). Normal structure, function, and histology of the spleen. *Toxicol. Pathol.* **34,** 455-465.

Chepelev, N. L., Moffat, I. D., Bowers, W. J., and Yauk, C. L. (2015a). Neurotoxicity may be an overlooked consequence of benzo[a]pyrene exposure that is relevant to human health risk assessment. *Mutation Research - Reviews in Mutation Research.* **764,** 64-89.

Chepelev, N., Moffat, I., Labib, S., Bourdon, J., Williams, A., Kuo, B., Buick, J., Lemieux, F., Malik, A., Halappanavar, S., and Yauk, C. (2015b). Integrating toxicogenomics into human health risk assessment: lessons learned from the benzo[*a*]pyrene case study. *Crit. Rev. Toxicol.* **45,** 44-52.

Chepelev, N. L., Kennedy, D. A., Gagné, R., White, T., Long, A. S., Yauk, C. L., and White, P. A. (2015c). HPLC Measurement of the DNA Oxidation Biomarker, 8-oxo-7,8-dihydro-2'-

deoxyguanosine, in Cultured Cells and Animal Tissues *Journal of Visualized Experiments.* e52697.

Chepelev, N. L. and Willmore, W. G. (2011). Regulation of iron pathways in response to hypoxia. *Free Radic. Biol. Med.* **50,** 645-666.

Committee on Carcinogenicity of Chemicals in Food, Consumer Products and the Environment. (2003). Available at: http://cot.food.gov.uk/sites/default/files/cot/cocsection03.pdf.

Cool, S. M. and Nurcombe, V. (2006). Heparan sulfate regulation of progenitor cell fate. *J. Cell. Biochem.* **99,** 1040-1051.

De Jong, W. H., Kroese, E. D., Vos, J. G., and Van Loveren, H. (1999). Detection of immunotoxicity of benzo[a]pyrene in a subacute toxicity study after oral exposure in rats. *Toxicological Sciences.* **50,** 214-220.

De Raat, W. K., Kooijman, S. A., and Gielen, J. W. (1987). Concentrations of polycyclic hydrocarbons in airborne particles in The Netherlands and their correlation with mutagenicity. *Sci. Total Environ.* **66,** 95-114.

Dertinger, S. D., Camphausen, K., Macgregor, J. T., Bishop, M. E., Torous, D. K., Avlasevich, S., Cairns, S., Tometsko, C. R., Menard, C., Muanza, T., Chen, Y., Miller, R. K., Cederbrant, K., Sandelin, K., Ponten, I., and Bolcsfoldi, G. (2004). Three-color labeling method for flow cytometric measurement of cytogenetic damage in rodent and human blood. *Environ. Mol. Mutagen.* **44,** 427-435.

Ding, W. X., Ni, H. M., Li, M., Liao, Y., Chen, X., Stolz, D. B., Dorn, G. W.,2nd, and Yin, X. M. (2010). Nix is critical to two distinct phases of mitophagy, reactive oxygen species-mediated autophagy induction and Parkin-ubiquitin-p62-mediated mitochondrial priming. *J. Biol. Chem.* **285,** 27879-27890.

Diwan, A., Koesters, A. G., Capella, D., Geiger, H., Kalfa, T. A., and Dorn, G. W.,2nd. (2008). Targeting erythroblast-specific apoptosis in experimental anemia. *Apoptosis.* **13,** 1022-1030.

Diwan, A., Koesters, A. G., Odley, A. M., Pushkaran, S., Baines, C. P., Spike, B. T., Daria, D., Jegga, A. G., Geiger, H., Aronow, B. J., Molkentin, J. D., Macleod, K. F., Kalfa, T. A., and Dorn, G. W.,2nd. (2007). Unrestrained erythroblast development in Nix-/- mice reveals a mechanism for apoptotic modulation of erythropoiesis. *Proc. Natl. Acad. Sci. U. S. A.* **104,** 6794-6799.

Dobin, A., Davis, C. A., Schlesinger, F., Drenkow, J., Zaleski, C., Jha, S., Batut, P., Chaisson, M., and Gingeras, T. R. (2013). STAR: ultrafast universal RNA-seq aligner. *Bioinformatics.* **29,** 15-21.

Durant, J. L., Busby, W. F.,Jr, Lafleur, A. L., Penman, B. W., and Crespi, C. L. (1996). Human cell mutagenicity of oxygenated, nitrated and unsubstituted polycyclic aromatic hydrocarbons associated with urban aerosols. *Mutat. Res.* **371,** 123-157.

Gao, J. and Burchiel, S. W. (2014). Genotoxic Mechanisms of PAH-Induced Immunotoxicity. *Molecular Immunotoxicology.* 245-262.

Gao, J., Lauer, F. T., Dunaway, S., and Burchiel, S. W. (2005). Cytochrome P450 1B1 is required for 7,12-dimethylbenz(a)-anthracene (DMBA) induced spleen cell immunotoxicity. *Toxicol. Sci.* **86,** 68-74.

Gao, J., Mitchell, L. A., Lauer, F. T., and Burchiel, S. W. (2008). p53 and ATM/ATR regulate 7,12-dimethylbenz[a]anthracene-induced immunosuppression. *Mol. Pharmacol.* **73,** 137-146.

Gossen, J. A., De Leeuw, W. J. F., Tan, C. H. T., Zwarthoff, E. C., Berends, F., Lohman, P. H. M., Knook, D. L., and Vijg, J. (1989). Efficient rescue of integrated shuttle vectors from transgenic mice: A model for studying mutations in vivo. *Proc. Natl. Acad. Sci. U. S. A.* **86,** 7971-7975.

Harper, T. A.,Jr, Morre, J., Lauer, F. T., McQuistan, T. J., Hummel, J. M., Burchiel, S. W., and Williams, D. E. (2015). Analysis of dibenzo[def,p]chrysene-deoxyadenosine adducts in wild-type and cytochrome P450 1b1 knockout mice using stable-isotope dilution UHPLC-MS/MS. *Mutat. Res. Genet. Toxicol. Environ. Mutagen.* **782,** 51-56.

Higginbotham, S., RamaKrishna, N. V., Johansson, S. L., Rogan, E. G., and Cavalieri, E. L. (1993). Tumor-initiating activity and carcinogenicity of dibenzo[a,l]pyrene versus 7,12-dimethylbenz[a]anthracene and benzo[a]pyrene at low doses in mouse skin. *Carcinogenesis.* **14,** 875-878.

Holladay, S. D. and Smith, B. J. (1995). Benzo[a]pyrene-induced alterations in total immune cell number and cell-surface antigen expression in the thymus, spleen and bone marrow of B6C3F1 mice. *Vet. Hum. Toxicol.* **37,** 99-104.

IARC Working Group on the Evaluation of Carcinogenic Risks to Humans. (2010). Some non-heterocyclic polycyclic aromatic hydrocarbons and some related exposures. *IARC Monogr. Eval. Carcinog. Risks Hum.* **92,** 1-853.

Imazu, T., Shimizu, S., Tagami, S., Matsushima, M., Nakamura, Y., Miki, T., Okuyama, A., and Tsujimoto, Y. (1999). Bcl-2/E1B 19 kDa-interacting protein 3-like protein (Bnip3L) interacts with bcl-2/Bcl-xL and induces apoptosis by altering mitochondrial membrane permeability. *Oncogene.* **18,** 4523-4529.

Jackson, A. F., Williams, A., Recio, L., Waters, M. D., Lambert, I. B., and Yauk, C. L. (2014). Case study on the utility of hepatic global gene expression profiling in the risk assessment of the carcinogen furan. *Toxicol. Appl. Pharmacol.* **274,** 63-77.

Kamath, A. T., Pooley, J., O'Keeffe, M. A., Vremec, D., Zhan, Y., Lew, A. M., D'Amico, A., Wu, L., Tough, D. F., and Shortman, K. (2000). The development, maturation, and turnover rate of mouse spleen dendritic cell populations. *J. Immunol.* **165,** 6762-6770.

Kolb, J. P., Poupon, M. F., Lespinats, G. M., Sabolovic, D., and Loisillier, F. (1977). Splenic modifications induced by cyclophosphamide in C3H/He, nude, and "B" mice. *J. Immunol.* **118,** 1595-1599.

Kupershmidt, I., Su, Q. J., Grewal, A., Sundaresh, S., Halperin, I., Flynn, J., Shekar, M., Wang, H., Park, J., Cui, W., Wall, G. D., Wisotzkey, R., Alag, S., Akhtari, S., and Ronaghi, M. (2010). Ontology-based meta-analysis of global collections of high-throughput public data. *PLoS One.* **5,** 10.1371/journal.pone.0013066.

Labib, S., Yauk, C., Williams, A., Arlt, V., Phillips, D. H., White, P., and Halappanavar, S. (2012). Sub-chronic oral exposure to benzo(a)pyrene leads to distinct transcriptomic changes in the lungs that are related to carcinogenesis. *Toxicol. Sci.* **129,** 213-234.

Langmead, B. and Salzberg, S. L. (2012). Fast gapped-read alignment with Bowtie 2. *Nat. Methods.* **9,** 357-359.

Lemieux, C. L., Douglas, G. R., Gingerich, J., Phonethepswath, S., Torous, D. K., Dertinger, S. D., Phillips, D. H., Arlt, V. M., and White, P. A. (2011). Simultaneous measurement of benzo[a]pyrene-induced Pig-a and lacZ mutations, micronuclei and DNA adducts in Muta Mouse. *Environ. Mol. Mutagen.* **52,** 756-765.

Li, H. H., Hyduke, D. R., Chen, R., Heard, P., Yauk, C. L., Aubrecht, J., and Fornace, A. J.,Jr. (2015). Development of a toxicogenomics signature for genotoxicity using a dose-optimization and informatics strategy in human cells. *Environ. Mol. Mutagen.* **56,** 505-519.

Malik, A. I., Rowan-Carroll, A., Williams, A., Lemieux, C. L., Long, A. S., Arlt, V. M., Phillips, D. H., White, P. A., and Yauk, C. L. (2013). Hepatic genotoxicity and toxicogenomic responses in MutaMouse males treated with dibenz[a,h]anthracene. *Mutagenesis.* **28,** 543-554.

Malik, A. I., Williams, A., Lemieux, C. L., White, P. A., and Yauk, C. L. (2012). Hepatic mRNA, microRNA, and miR-34a-target responses in mice after 28 days exposure to doses of benzo(a)pyrene that elicit DNA damage and mutation. *Environ. Mol. Mutagen.* **53,** 10-21.

Mancias, J. D., Wang, X., Gygi, S. P., Harper, J. W., and Kimmelman, A. C. (2014). Quantitative proteomics identifies NCOA4 as the cargo receptor mediating ferritinophagy. *Nature.* **509,** 105-109.

Mebius, R. E. and Kraal, G. (2005). Structure and function of the spleen. *Nat. Rev. Immunol.* **5,** 606-616.

Meek, M. E., Boobis, A., Cote, I., Dellarco, V., Fotakis, G., Munn, S., Seed, J., and Vickers, C. (2014). New developments in the evolution and application of the WHO/IPCS framework on mode of action/species concordance analysis. *J. Appl. Toxicol.* **34,** 1-18.

Moffat, I., Chepelev, N., Labib, S., Bourdon-Lacombe, J., Kuo, B., Buick, J. K., Lemieux, F., Williams, A., Halappanavar, S., Malik, A., Luijten, M., Aubrecht, J., Hyduke, D. R., Fornace, A. J. J., Swartz, C. D., Recio, L., and Yauk, C. L. (2015). Comparison of toxicogenomics and traditional approaches to inform mode of action and points of departure in human health risk assessment of benzo[*a*]pyrene in drinking water. *Crit. Rev. Toxicol.* **45,** 1-43.

Nakatsuru, Y., Wakabayashi, K., Fujii-Kuriyama, Y., Ishikawa, T., Kusama, K., and Ide, F. (2004). Dibenzo[A,L]pyrene-induced genotoxic and carcinogenic responses are dramatically suppressed in aryl hydrocarbon receptor-deficient mice. *Int. J. Cancer.* **112,** 179-183.

Organisation for Economic Co-operation and Development (OECD). (2008). Test No. 407: Repeated Dose 28-day Oral Toxicity Study in Rodents. http://www.oecd-ilibrary.org/

Petroianu, A. (2007). Drug-induced splenic enlargement. *Expert Opin. Drug Saf.* **6,** 199-206.

Phillips, D. H. and Arlt, V. M. (2007). The 32P-postlabeling assay for DNA adducts. *Nat. Protoc.* **2,** 2772-2781.

Ramesh, A., Walker, S. A., Hood, D. B., Guillen, M. D., Schneider, K., and Weyand, E. H. (2004). Bioavailability and risk assessment of orally ingested polycyclic aromatic hydrocarbons. *Int. J. Toxicol.* **23,** 301-333.

R-Development-Core-Team. (2010). R: A Language and Environment for Statistical Computing. *R Foundation for Statistical Computing, Vienna, Austria.* http://www.lsw.uni-heidelberg.de/users/christlieb/teaching/UKStaSS10/R-refman.pdf.

Ren, F., Su, F., Ning, H., Wang, Y., Geng, Y., Feng, Y., Wang, Y., Zhang, Y., Jin, Z., Li, Y., Jia, B., and Chang, Z. (2013). SIPAR negatively regulates STAT3 signaling and inhibits progression of melanoma. *Cell. Signal.* **25,** 2272-2280.

Robinson, M. D., McCarthy, D. J., and Smyth, G. K. (2010). edgeR: a Bioconductor package for differential expression analysis of digital gene expression data. *Bioinformatics.* **26,** 139-140.

Robinson, M. D. and Oshlack, A. (2010). A scaling normalization method for differential expression analysis of RNA-seq data. *Genome Biol.* **11,** R25-2010-11-3-r25.

Safran, M., Dalah, I., Alexander, J., Rosen, N., Iny Stein, T., Shmoish, M., Nativ, N., Bahir, I., Doniger, T., Krug, H., Sirota-Madi, A., Olender, T., Golan, Y., Stelzer, G., Harel, A., and Lancet, D. (2010). GeneCards Version 3: the human gene integrator. *Database (Oxford).* **2010,** baq020.

Shimada, T. and Fujii-Kuriyama, Y. (2004). Metabolic activation of polycyclic aromatic hydrocarbons to carcinogens by cytochromes P450 1A1 and 1B1. *Cancer. Sci.* **95,** 1-6.

Siddens, L. K., Larkin, A., Krueger, S. K., Bradfield, C. A., Waters, K. M., Tilton, S. C., Pereira, C. B., Löhr, C. V., Arlt, V. M., Phillips, D. H., Williams, D. E., and Baird, W. M. (2012). Polycyclic aromatic hydrocarbons as skin carcinogens: Comparison of benzo[a]pyrene, dibenzo[def,p]chrysene and three environmental mixtures in the FVB/N mouse. *Toxicol. Appl. Pharmacol.* **264,** 377-386.

Tao, Y., Wu, Q., Guo, X., Zhang, Z., Shen, Y., and Wang, F. (2014). MBD5 regulates iron metabolism via methylation-independent genomic targeting of Fth1 through KAT2A in mice. *Br. J. Haematol.* **166,** 279-291.

Thomas, R. S., Clewell III, H. J., Allen, B. C., Wesselkamper, S. C., Wang, N. C. Y., Lambert, J. C., Hess-Wilson, J. K., Zhao, Q. J., and Andersen, M. E. (2011). Application of transcriptional benchmark dose values in quantitative cancer and noncancer risk assessment. *Toxicological Sciences.* **120,** 194-205.

US Department of Health and Human Sciences. (2014). National Toxicology Program. Micronucleus. **2014**.

White, P. A. (2002). The genotoxicity of priority polycyclic aromatic hydrocarbons in complex mixtures. *Mutat. Res.* **515,** 85-98.

Wohak, L. E., Krais, A. M., Kucab, J. E., Stertmann, J., Øvrebø, S., Seidel, A., Phillips, D. H., and Arlt, V. M. (2014). Carcinogenic polycyclic aromatic hydrocarbons induce CYP1A1 in human cells via a p53-dependent mechanism. *Arch. Toxicol.* doi:10.1007/s00204-014-1409-1.

Wu, H., Kerr, K. K., Cui, X., and Churchill, G. A. (2003). MAANOVA: A software package for the analysis of spotted cDNA microarray experiments. In The Analysis of Gene Expression Data: Methods and Software. (G. Parmigiani, E. S. Garrett, R. A. Irizarry, and S. L. Zeger, Eds.)pp 313-341. Springer, New York.

Yang, L., Allen, B. C., and Thomas, R. S. (2007). BMDExpress: A software tool for the benchmark dose analyses of genomic data. *BMC Genomics.* **8,** 387.

Yang, Y. H., Dudoit, S., Luu, P., Lin, D. M., Peng, V., Ngai, J., and Speed, T. P. (2002). Normalization for cDNA microarray data: a robust composite method addressing single and multiple slide systematic variation. Nucleic Acids Res. **30,** e15.

Zhang, J., Loyd, M. R., Randall, M. S., Waddell, M. B., Kriwacki, R. W., and Ney, P. A. (2012). A short linear motif in BNIP3L (NIX) mediates mitochondrial clearance in reticulocytes. *Autophagy.* **8,** 1325-1332.